



Paeonol promotes Opa1-mediated mitochondrial fusion via activating the CK2 α -Stat3 pathway in diabetic cardiomyopathy

Chaoyang Liu^{a,b,c,1}, Yuehu Han^{d,1}, Xiaoming Gu^{b,1}, Man Li^{b,c}, Yanyan Du^{b,c}, Na Feng^b, Juan Li^b, Shumiao Zhang^b, Leonid N. Maslov^e, Guoen Wang^a, Jianming Pei^{b,*}, Feng Fu^{b,**}, Mingge Ding^{a,***}

^a Department of Geriatrics Cardiology, The Second Affiliated Hospital, School of Medicine, Xi'an Jiaotong University, Xi'an, Shaanxi, 710004, China

^b Department of Physiology and Pathophysiology, National Key Discipline of Cell Biology, Fourth Military Medical University, Xi'an, Shaanxi, 710032, China

^c School of Life Science, Northwest University, Xi'an, Shaanxi, 710069, China

^d Department of Cardiovascular Surgery, Xijing Hospital, Fourth Military Medical University, Xi'an, Shaanxi, 710032, China

^e Cardiology Research Institute, Tomsk National Research Medical Center of the Russian Academy of Science, Tomsk, 634000, Russia

ARTICLE INFO

Keywords:

Diabetic cardiomyopathy
Paeonol
Mitochondrial fusion
CK2 α
Stat3
Opa1

ABSTRACT

Diabetes disrupts mitochondrial function and often results in diabetic cardiomyopathy (DCM). Paeonol is a bioactive compound that has been reported to have pharmacological potential for cardiac and mitochondrial protection. This study aims to explore the effects of paeonol on mitochondrial disorders in DCM and the underlying mechanisms. We showed that paeonol promoted Opa1-mediated mitochondrial fusion, inhibited mitochondrial oxidative stress, and preserved mitochondrial respiratory capacity and cardiac performance in DCM *in vivo* and *in vitro*. Knockdown of Opa1 blunted the above protective effects of paeonol in both diabetic hearts and high glucose-treated cardiomyocytes. Mechanistically, inhibitor screening, siRNA knockdown and chromatin immunoprecipitation experiments showed that paeonol-promoted Opa1-mediated mitochondrial fusion required the activation of Stat3, which directly bound to the promoter of Opa1 to upregulate its transcriptional expression. Moreover, pharmmapper screening and molecular docking studies revealed that CK2 α served as a direct target of paeonol that interacted with Jak2 and induced the phosphorylation and activation of Jak2-Stat3. Knockdown of CK2 α blunted the promoting effect of paeonol on Jak2-Stat3 phosphorylation and Opa1-mediated mitochondrial fusion. Collectively, we have demonstrated for the first time that paeonol is a novel mitochondrial fusion promoter in protecting against hyperglycemia-induced mitochondrial oxidative injury and DCM at least partially via an Opa1-mediated mechanism, a process in which paeonol interacts with CK2 α and restores its kinase activity that subsequently increasing Jak2-Stat3 phosphorylation and enhancing the transcriptional level of Opa1. These findings suggest that paeonol or the promotion of mitochondrial fusion might be a promising strategy for the treatment of DCM.

1. Introduction

The incidence of diabetes has been rapidly increasing throughout the world. Cardiovascular complications are major causes of morbidity and mortality in diabetic patients [1]. Among these complications, diabetic cardiomyopathy (DCM) is a diabetes-associated heart disease that is independent of coronary artery disease and hypertension [2]. DCM is

characterized by abnormalities in cardiac structure and function including myocardial hypertrophy, interstitial fibrosis, cardiomyocyte apoptosis, and diastolic and systolic dysfunction [3]. These characteristics of DCM lead to heart failure, contributing to increased morbidity and mortality of in patients with diabetes [4]. Currently, the availability of effective therapeutic interventions against DCM is limited.

The heart is an organ with high energy demand, largely dependent

* Corresponding author.

** Corresponding author. Department of Physiology and Pathophysiology, National Key Discipline of Cell Biology, Fourth Military Medical University.

*** Corresponding author. Department of Geriatrics Cardiology, The Second Affiliated Hospital, School of Medicine, Xi'an Jiaotong University.

E-mail addresses: jmpei8@fmmu.edu.cn (J. Pei), fufeng048@126.com (F. Fu), dingmingge@xjtu.edu.cn (M. Ding).

¹ Chaoyang Liu, Yuehu Han and Xiaoming Gu contributed equally to this article.

<https://doi.org/10.1016/j.redox.2021.102098>

Received 15 June 2021; Received in revised form 29 July 2021; Accepted 7 August 2021

Available online 10 August 2021

2213-2317/© 2021 The Authors.

Published by Elsevier B.V. This is an open access article under the CC BY-NC-ND license

(<http://creativecommons.org/licenses/by-nc-nd/4.0/>).

on the function of mitochondria, which provide approximately 90% energy and are a major source of reactive oxygen species (ROS) [5]. Increased mitochondrial ROS production and resultant mitochondrial dysfunction are generally recognized to play a pivotal role in the development of DCM [6,7]. Recently, it has been highlighted that imbalanced mitochondrial fusion/fission dynamics is an early component that increases mitochondrial ROS production and induces mitochondrial dysfunction [8,9]. Diabetic hearts display excessive mitochondrial fission and inhibited mitochondrial fusion. Our previous studies have found that correcting mitochondrial dynamics by moderately inhibiting mitochondrial fission or enhancing mitochondrial fusion inhibits mitochondria-derived ROS generation and mitigates mitochondrial dysfunction in diabetic hearts or high glucose-treated cardiomyocytes [10,11]. Of note, the study by Qin et al. has shown that promoting mitochondrial fusion by fusion protein Mfn2 overexpression does not impair cardiac mitochondrial function, whereas completely inhibiting Drp1-mediated mitochondrial fission impairs mitochondrial quality at baseline [12]. This suggests that mitochondrial fusion promotion is a more safe strategy than mitochondrial fission inhibition to maintain cardiac mitochondrial function. Hence, the discovery of safe and effective pharmacotherapy targeting mitochondrial fusion promotion is meaningful for the treatment of DCM.

Paenol (Pae) is a bioactive compound extracted from the root of *Paeonia albiflora* and has a long history of clinical use. Currently, the dosage forms of Pae approved by the Food and Drug Administration of China for human use include tablets, injections and ointments. Oral and injection administrations of Pae are effective in relieving inflammation/pain-related diseases, such as rheumatoid arthritis, headache, and muscle pain [13]. Moreover, Pae has been reported to have great pharmacological potential for cardiac and mitochondrial protection. Indeed, it has been shown that Pae reduces ischemia-induced myocardial apoptosis by inhibiting oxidative stress [14,15] and attenuates glutamate-induced mitochondrial injury by restoring mitochondrial membrane potential and inhibiting cytochrome c release [16], suggesting Pae has a protective effect on the mitochondria. Given that the promotion of mitochondrial fusion is crucial in maintaining mitochondrial homeostasis and normal cardiac function, investigating whether Pae is an efficient mitochondrial fusion promoter in a DCM model is worthwhile. In the present study, we explored the effects of Pae on cardiac pathology and mitochondrial fusion/fission dynamics in diabetic hearts *in vivo* and in hyperglycemia-treated primary cardiomyocytes *in vitro*, with a specific focus on the molecular mechanisms of how Pae promotes mitochondrial fusion. Our results have revealed that Pae is a novel mitochondrial fusion promoter in protecting against DCM through the CK2 α -Stat3-Opa1 signaling pathway.

2. Materials and methods

An extended “Materials and Methods” is provided in the Supplementary Materials and Methods.

2.1. Cardiomyocyte culture and treatment

Primary neonatal cardiomyocytes were isolated from 1-2-day-old neonatal Sprague-Dawley rats. The cardiomyocytes were subjected to normal glucose (5.5 mmol/L, NG) or high glucose (33 mmol/L, HG) challenge for 48 h with the vehicle or various concentrations of Pae supplement. Pae (catalog number: MB1762-S, purity > 98%) was obtained from Dalian Meilun Biology Technology (Dalian, China).

2.2. Assessment of mitochondrial morphology, ROS and ATP in cardiomyocytes

The mitochondria in the primary cardiomyocytes were labeled with MitoTracker Red CMXRos probe (100 nmol/L, Invitrogen, Carlsbad, USA) and imaged using a confocal laser-scanning microscope (Nikon

A1R MP + Confocal Microscope). The number and volume of the mitochondria observed were analyzed and quantified as previously described [17]. After MitoTracker Red staining, flow cytometry was performed to analyze mitochondrial mass. MitoSOX staining (Invitrogen, Carlsbad, USA) was performed to evaluate mitochondrial ROS levels in cardiomyocytes. Intracellular ATP content was detected using an ATP bioluminescent assay kit (Biovision, California, USA) according to the manufacturer's protocol.

2.3. Animal experimental design and treatment

All animal experimental procedures were conducted in accordance with the National Institutes of Health Guidelines for the Care and Use of Laboratory Animals (8th Edition, 2011) and the study was approved by the Fourth Military Medical University Ethics Committee. Sixty-five male 6–8-week-old Sprague-Dawley rats were obtained and maintained under controlled conditions of temperature (22 ± 2 °C) and a 12-h light/dark cycle. Diabetes was induced by a single intraperitoneal injection of streptozotocin (STZ, Sigma-Aldrich, 65 mg/kg) dissolved in 0.1 mol/l citrate buffer (pH 4.5) [18]. Control animals received an intraperitoneal injection of vehicle (citrate buffer) only. One week after STZ injection, the rats with fasting glycemia levels ≥ 11.1 mM were considered diabetic. After confirmation of diabetes, the rats were administered with the vehicle or Pae (catalog number: MB1762, purity > 98%, Dalian Meilun Biology Technology, China) respectively for an additional 12 weeks. Pae was mixed with the vehicle (0.5% sodium carboxymethyl cellulose) and then administered to the animals by oral gastric gavage at 75, 150 or 300 mg/kg/day based on previous studies [19,20].

2.4. Prediction of potential targets of Pae and molecular docking

The SDF (Structure Data File) file of Pae was downloaded from PubChem (<https://pubchem.ncbi.nlm.nih.gov/compound/11092>, accessed by October 15, 2020) and the effective targets were predicted using the PharmMapper Server (<http://www.lilab-ecust.cn/pharmmapper/>) by employing “All Targets” model [21,22]. The submission ID was recorded during the operation. Autodock Vina 1.1.2 was employed to investigate the binding affinity and binding sites between Pae and CK2 α . Briefly, the SDF file of Pae was converted into PDBQT format by using AutoDock Tools. The 3D crystal structure of the CK2 α kinase complex was obtained from the Protein Data Bank (PDB) (<http://www.rcsb.org>, PDB ID: 1M2P). The search grid of CK2 was identified as center_x: 23.331, center_y: 6.252 and center_z: 18.182 with dimensions size_x: 15, size_y: 15, and size_z: 15. The docking protocol was generated as described previously [23,24]. The Promega CK2 α Kinase Assay kit was utilized to explore the effects of Pae on the activity of CK2 α according to the manufacturer's instructions.

2.5. Western blot analysis

Total protein from rat hearts and the cardiomyocytes was extracted by using RIPA buffer containing protease inhibitor cocktail. The standard Western blotting method was used as previously described [25]. Detailed information for Western blotting is available in the Supplementary Materials and Methods section. The antibodies used were shown in [Supplementary Table 1](#) in the Supplementary Materials and Methods.

2.6. Statistical analysis

All values were presented as the mean \pm standard error of the mean (SEM). Data were analyzed by one-way ANOVA followed by Tukey's post-hoc test using GraphPad Prism software (version 8.0). Differences with P values less than 0.05 were considered to be statistically significant.

3. Results

3.1. Pae promoted mitochondrial fusion and improved mitochondrial function in high glucose-treated cardiomyocytes

The cardiomyocytes were treated with Pae at 25, 50, 100 and 200 $\mu\text{mol/L}$ for 48 h. As shown in [Supplementary Fig. S1](#), the CCK8 assay showed that only 200 $\mu\text{mol/L}$ Pae slightly inhibited cell viability, while the other concentrations of Pae had no significant effect on cell viability in the cardiomyocytes. Therefore, 100 $\mu\text{mol/L}$ of Pae was considered to be the safest concentration. In light of the results from previous studies [26,27], this concentration was used to explore the effects of Pae on mitochondrial homeostasis including mitochondrial dynamics and biogenesis in primary cardiomyocytes. As shown in [Fig. 1a](#), the mitochondria of the NG-cultured cardiomyocytes appeared as elongated tubules with highly interconnected networks. When subjected to HG medium, the mitochondria became spherical and shorter. Compared to NG-cultured cardiomyocytes, decreased mitochondrial volume and

increased number of mitochondria were observed in the HG-cultured cardiomyocytes ([Fig. 1a–c](#)). Treatment with Pae resulted in a significant increase in the mitochondrial volume and a significant decrease in the number of mitochondria in the HG-cultured cardiomyocytes ([Fig. 1a–c](#)), indicating that Pae promoted mitochondrial fusion in hyperglycemia-treated primary cardiomyocytes. Mitochondrial biogenesis was determined by measuring the relative mtDNA content and the MitoTracker Red stained mitochondrial mass using quantitative real-time PCR and flow cytometry respectively. HG or Pae induced no changes in the mtDNA content and the mitochondrial mass in cardiomyocytes ([Fig. 1d](#) and [e](#)), suggesting that Pae did not enhance mitochondrial biogenesis. Moreover, compared to the NG-cultured cardiomyocytes, the HG-cultured cardiomyocytes exhibited elevated mitochondria-derived superoxide production (as detected by MitoSOX staining in [Fig. 1g](#)), reduced ATP production ([Fig. 1f](#)), and suppressed mitochondrial respiratory capacities including maximal respiration and spare respiratory capacity ([Fig. 1h](#) and [i](#)). Treatment with Pae significantly reduced mitochondria-derived superoxide production, increased

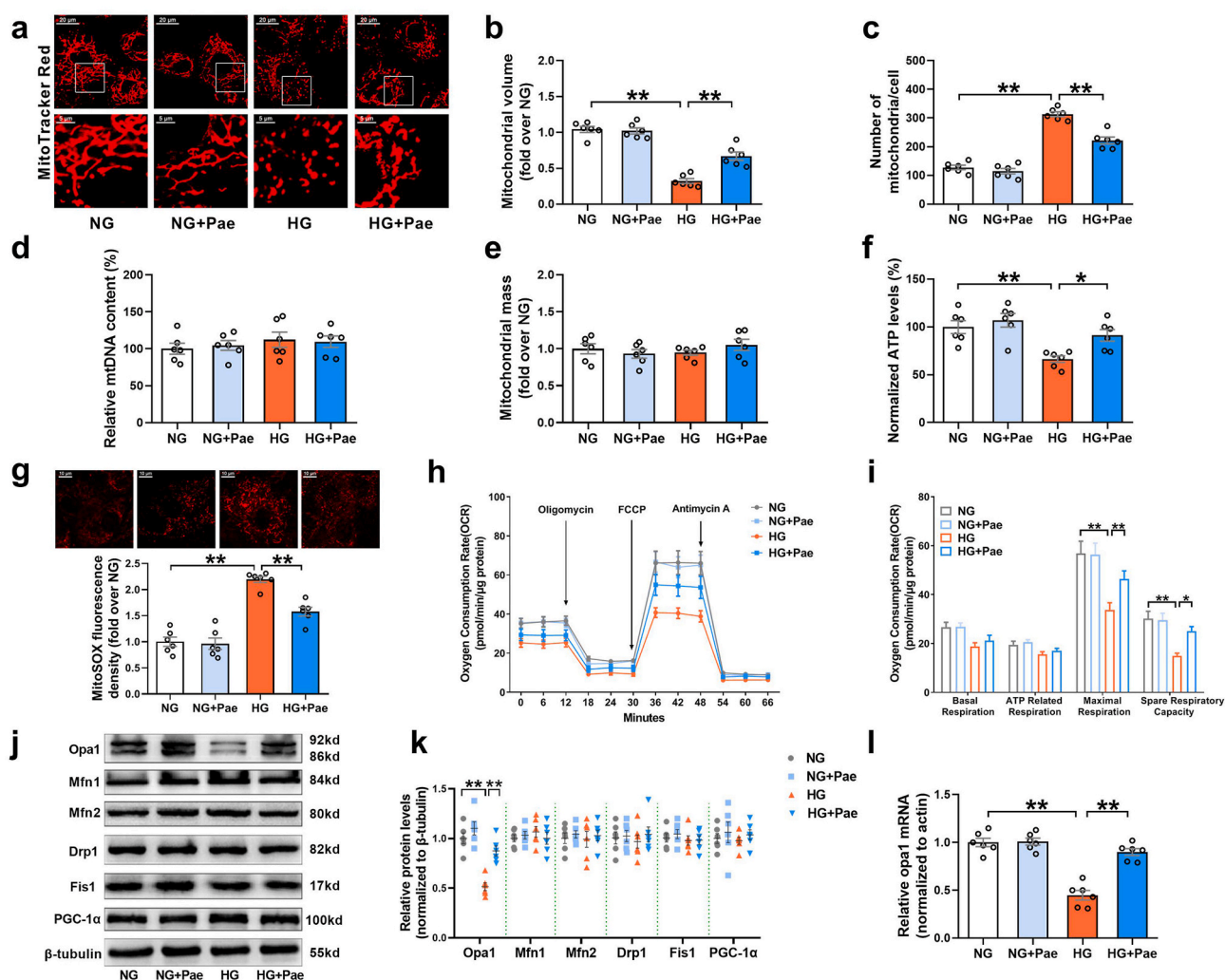


Fig. 1. Pae promoted Opa1-related mitochondrial fusion and enhanced mitochondrial respiratory capacity in high glucose (HG)-treated cardiomyocytes. (a) Representative confocal microscope images of mitochondrial morphology stained by MitoTracker Red. Original magnification $\times 600$. (b) Quantification of mean mitochondrial volume. (c) Quantification of mitochondrial number per cell. (d) mtDNA content normalized to nuclear DNA content. (e) Quantification of mitochondrial mass. (f) Quantification of normalized ATP levels. (g) Representative images and quantitative analysis of MitoSOX-stained mitochondria-derived superoxide production. (h–i) Oxygen consumption rate (OCR) measured by Seahorse and quantitative statistical analysis of OCR. (j–k) Representative blots and quantitative analysis of the mitochondrial fission/fusion-related proteins including Opa1, Mfn1, Mfn2, Drp1 and Fis1. (l) Quantitative analysis of Opa1 mRNA expression determined by real-time PCR. Values are the means \pm SEM. NG, normal glucose (5.5 mmol/L); HG, high glucose (33 mmol/L); Pae, paeonol (100 $\mu\text{mol/L}$). $n = 6$ in each group. All data are shown as means \pm SEM. * $P < 0.05$, ** $P < 0.01$. (For interpretation of the references to colour in this figure legend, the reader is referred to the Web version of this article.)

ATP production, and recovered the mitochondrial respiratory capacity in the HG-treated cardiomyocytes (Fig. 1f–i).

Next, the expression patterns of mitochondrial fission/fusion proteins and PGC-1 α (a central regulator of mitochondrial biogenesis) were analyzed. Of the mitochondrial fission and fusion proteins (fission proteins: Drp1 and Fis1; fusion proteins: Mfn1, Mfn2 and Opa1), only the expression of Opa1 was significantly lower in the HG-treated cardiomyocytes than in the NG-cultured cardiomyocytes (Fig. 1j and k). Pae significantly reversed the decrease in Opa1 protein expression in the HG-cultured cardiomyocytes (Fig. 1j and k). No significant differences in PGC-1 α levels were observed among the experimental groups (Fig. 1j and k). Meanwhile, Pae mitigated the HG-induced reduction in Opa1 mRNA expression (Figure 1l), suggesting that the expression of Opa1

may be regulated at the transcriptional level (mRNA level). Taken together, these results indicate that Pae had no significant effect on PGC-1 α -related mitochondrial biogenesis in cardiomyocytes. Rather, Pae treatment enhanced the transcription of Opa1 and promoted mitochondrial fusion as well as mitochondrial function under hyperglycemic conditions in cardiomyocytes.

3.2. Pae-induced Opa1 upregulation was responsible for promoting mitochondrial fusion and function in HG-treated cardiomyocytes

We subsequently explored whether the upregulation of Opa1 expression was responsible for the mitochondrial protective effects of Pae. As shown in Fig. 2, knockdown of Opa1 with small interfering (si)

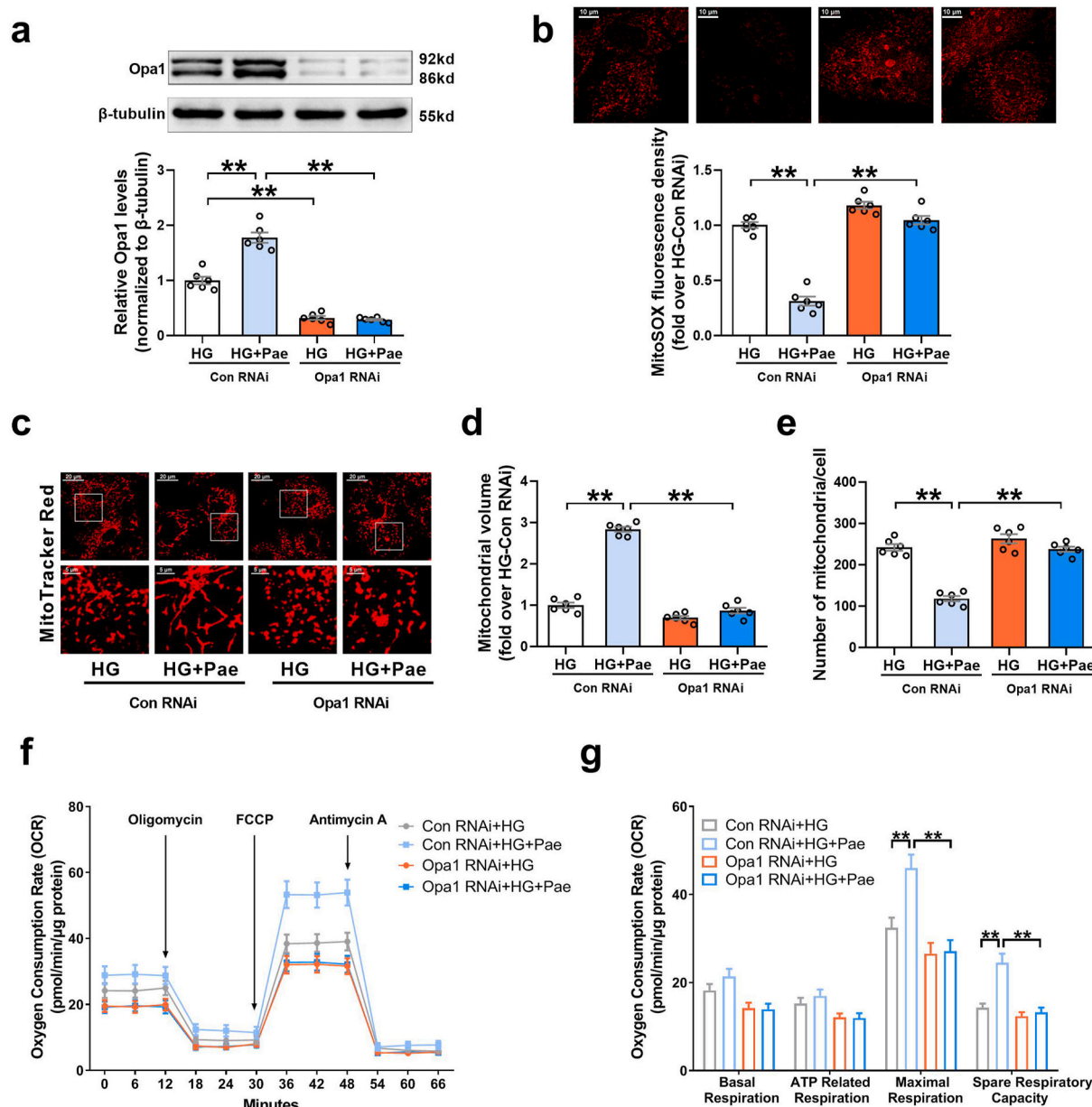


Fig. 2. Knockdown of Opa1 with siRNA blunted the inhibitory effects of Pae on mitochondrial oxidative stress and abrogated the promoting effects of Pae on mitochondrial fusion as well as mitochondrial respiratory capacity in high glucose (HG)-treated cardiomyocytes. (a) Representative blots and quantitative analysis of Opa1 expression. (b) Representative images and quantitative analysis of MitoSOX-stained mitochondria-derived superoxide production. (c) Representative confocal microscope images of mitochondrial morphology stained by MitoTracker Red. Original magnification $\times 600$. (d) Quantification of mean mitochondrial volume. (e) Quantification of mitochondrial number per cell. (f–g) Oxygen consumption rate (OCR) measured by Seahorse and quantitative statistical analysis of OCR. HG, high glucose (33 mmol/L); Pae, paeonol (100 μ mol/L). $n = 6$ in each group. All data are shown as means \pm SEM. $**P < 0.01$. (For interpretation of the references to colour in this figure legend, the reader is referred to the Web version of this article.)

RNA blunted the inhibitory effects of Pae on mitochondrial oxidative stress (Fig. 2a–b) and largely abrogated the promoting effects of Pae on mitochondrial fusion (Fig. 2c–e) as well as mitochondrial respiratory capacity in HG-treated cardiomyocytes (Fig. 2f–g). On the other hand, upregulation of Opa1 by transfecting with the adenovirus encoding Opa1 (Ad-Opa1) alone efficiently inhibited mitochondrial oxidative stress and promoted mitochondrial fusion as well as mitochondrial respiratory capacity in HG-treated cardiomyocytes (Supplementary Fig. S2). These data indicated that the mitochondrial protective effects of Pae were largely dependent on the upregulation of Opa1.

3.3. Pae alleviated diabetic cardiomyopathy in the rats

Since the data suggest that Pae was an efficient mitochondrial fusion promoter against hyperglycemia-induced mitochondrial oxidative injury *in vitro*, the effects of Pae on diabetic hearts were then explored *in vivo*. As shown in Table 1, compared with the control rats, the diabetic rats had decreased body weight as well as increased blood glucose and serum total cholesterol (TC) and triacylglycerol (TG) levels. All doses of Pae had no significant effects on body weight or blood glucose in the diabetic rats. Pae significantly reduced serum TC levels of diabetic rats at doses of 150 or 300 mg/kg/d. The diabetic rats showed decreased left ventricular ejection fraction (LVEF) and left ventricular fraction shortening (LVFS) and increased left ventricular end-systolic diameter (LVESD) (Fig. 3a–d). The diabetic rats that received Pae supplementation at doses of 150 or 300 mg/kg/d but not 75 mg/kg/d showed increased LVEF and LVFS and decreased LVESD (Fig. 3a–d). There were no significant differences in the left ventricular end-diastolic diameter (LVEDD) among all the groups (Fig. 3a and e). Moreover, the diabetic rats that received Pae treatment at a dose of 300 mg/kg/day showed improved diastolic function as evidenced by increased E/A ratio (Fig. 3f and g). A previous study has shown that Pae was detected at concentrations around 1 µg/ml (6 µmol/L) in plasma after oral administration of moutan cortex decoction (Moutan cortex is the root bark of *Paeonia suffruticosa*. Moutan cortex decoction is the water extraction of moutan cortex.) containing 20 mg/kg paeonol [28]. It is estimated that blood concentrations of 45 or 90 µmol/L Pae may be approximately reached after oral administration of 150 mg/kg or 300 mg/kg paeonol respectively. Since 100 µmol/L Pae was validated in our experiments on cardiomyocytes, 300 mg/kg/day Pae was considered to be the optimal dose for the animal experiments to yield similar action and was denoted as Con + Pae or DM + Pae group for subsequent experiments. Hemodynamic measurements indicated that the LVSP (left ventricular systolic pressure) and \pm LV dp/dt_{max} (maximal and minimal first derivative of left ventricular pressure) were decreased, while the LVEDP (left ventricular end-diastolic pressure) was increased in the diabetic rats compared with the control rats (Fig. 3h–k). The diabetic rats that received Pae treatment at a dose of 300 mg/kg/day (DM + Pae) showed increased LVSP and \pm LV dp/dt_{max} and decreased LVEDP (Fig. 3h–k).

Cardiac hypertrophy and interstitial fibrosis are important characteristic changes in DCM. Compared with the control rats, the diabetic rats showed significant cardiac hypertrophy and interstitial fibrosis, as evidenced by increased cardiomyocyte cross-sectional area and collagen

volume fraction (Fig. 4a–c). Treatment with Pae significantly inhibited cardiac hypertrophy and interstitial fibrosis in the diabetic rats, as evidenced by decreased cardiomyocyte cross-sectional area and reduced collagen volume fraction (Fig. 4a–c). Oxidative stress and cardiomyocyte apoptosis have been implicated in the pathogenesis of DCM. As expected, there were increased cardiomyocyte apoptosis (indicated by apoptosis index and the expression of apoptosis-related proteins including cleaved caspase 3, Bax and anti-apoptosis protein Bcl2 in Fig. 4d–g) and oxidative stress (indicated by DHE staining, MnSOD expression and the GPx and MDA content in Fig. 4h–l) in the diabetic hearts compared with the control hearts. Pae treatment significantly reduced cardiomyocyte apoptosis and inhibited myocardial oxidative stress in the diabetic hearts (Fig. 4d–l). These results indicated that Pae mitigated diabetes-induced oxidative stress and apoptosis and improved cardiac structure and function in diabetic animals.

3.4. Pae promoted mitochondrial fusion and the restoration of mitochondrial function in diabetic hearts

The effects of Pae on mitochondrial dynamics were further validated *in vivo*. Mitochondrial size and number were determined to evaluate the fusion of mitochondria. In the diabetic hearts, the percentage of mitochondria with sizes $<0.6 \mu\text{m}^2$ was markedly higher, while the percentage of mitochondria with sizes of $0.6\text{--}1 \mu\text{m}^2$ or $>1 \mu\text{m}^2$ was significantly lower than that in the control hearts (Fig. 5a and b). Moreover, the mean mitochondrial size was smaller in the diabetic hearts than in the control hearts (Fig. 5a and c). Pae treatment promoted mitochondrial fusion in the diabetic hearts, as reflected by the reduced percentage of mitochondria with sizes $<0.6 \mu\text{m}^2$, an elevated percentage of mitochondria with sizes of $0.6\text{--}1 \mu\text{m}^2$ or $>1 \mu\text{m}^2$, and increased mean mitochondrial size (Fig. 5a, b, and 5c). No significant differences in the number of mitochondria per μm^2 were observed among the experimental groups (Fig. 5d). Pae treatment reversed the decrease in ATP levels in the diabetic hearts (Fig. 5e). Moreover, cristae density was significantly reduced in the diabetic hearts compared with that in the control hearts. Pae treatment increased the cristae density in the diabetic hearts (Fig. 5f–g).

Next, the expression patterns of mitochondrial fission/fusion proteins, PGC-1 α and mitochondrial respiratory chain complex I–V were analyzed. Of the mitochondrial fission and fusion proteins, only the expression of fusion-related protein Opa1 was also significantly lower in the diabetic hearts than in the control hearts (Fig. 5h and i). Pae administration attenuated the decrease in Opa1 expression (Fig. 5h and i). No significant differences in PGC-1 α and mitochondrial complexes II, III, IV (CII, CIII, CIV) were observed among the experimental groups (Fig. 5j and k). The expressions of mitochondrial complexes I and V were significantly reduced in the diabetic hearts, both of which were partially restored by Pae treatment (Fig. 5j and k). Pae also reversed the decrease in the mRNA expression of Opa1, complex I and V in the diabetic hearts (Figure 5l). Together, these data indicated that Pae promoted Opa1-related mitochondrial fusion and mitochondrial function in diabetic hearts.

Table 1

Basic characteristics of animals.

Groups	Con	Con + Pae (300 mg/kg)	DM	DM + Pae (75 mg/kg)	DM + Pae (150 mg/kg)	DM + Pae (300 mg/kg)
Body weight (g)	553.4 ± 17.6	543.3 ± 13.9	299.5 ± 12.6**	319.0 ± 11.5	317.8 ± 19.0	323.3 ± 19.5
Blood glucose (mmol/L)	5.01 ± 0.06	5.21 ± 0.14	21.3 ± 1.17**	22.0 ± 0.46	22.3 ± 0.41	22.5 ± 0.44
Serum TC (mmol/L)	1.15 ± 0.06	1.31 ± 0.03	1.82 ± 0.08**	1.77 ± 0.05	1.36 ± 0.09##	1.16 ± 0.07##
Serum TG (mmol/L)	0.40 ± 0.07	0.49 ± 0.07	1.56 ± 0.40**	1.56 ± 0.12	1.37 ± 0.14	0.91 ± 0.13

Values presented are mean ± SEM. Con, control; DM, diabetes mellitus; TC, total cholesterol; TG, triacylglycerol. n = 8. **P < 0.01 vs. Con; ##P < 0.01 vs. DM.

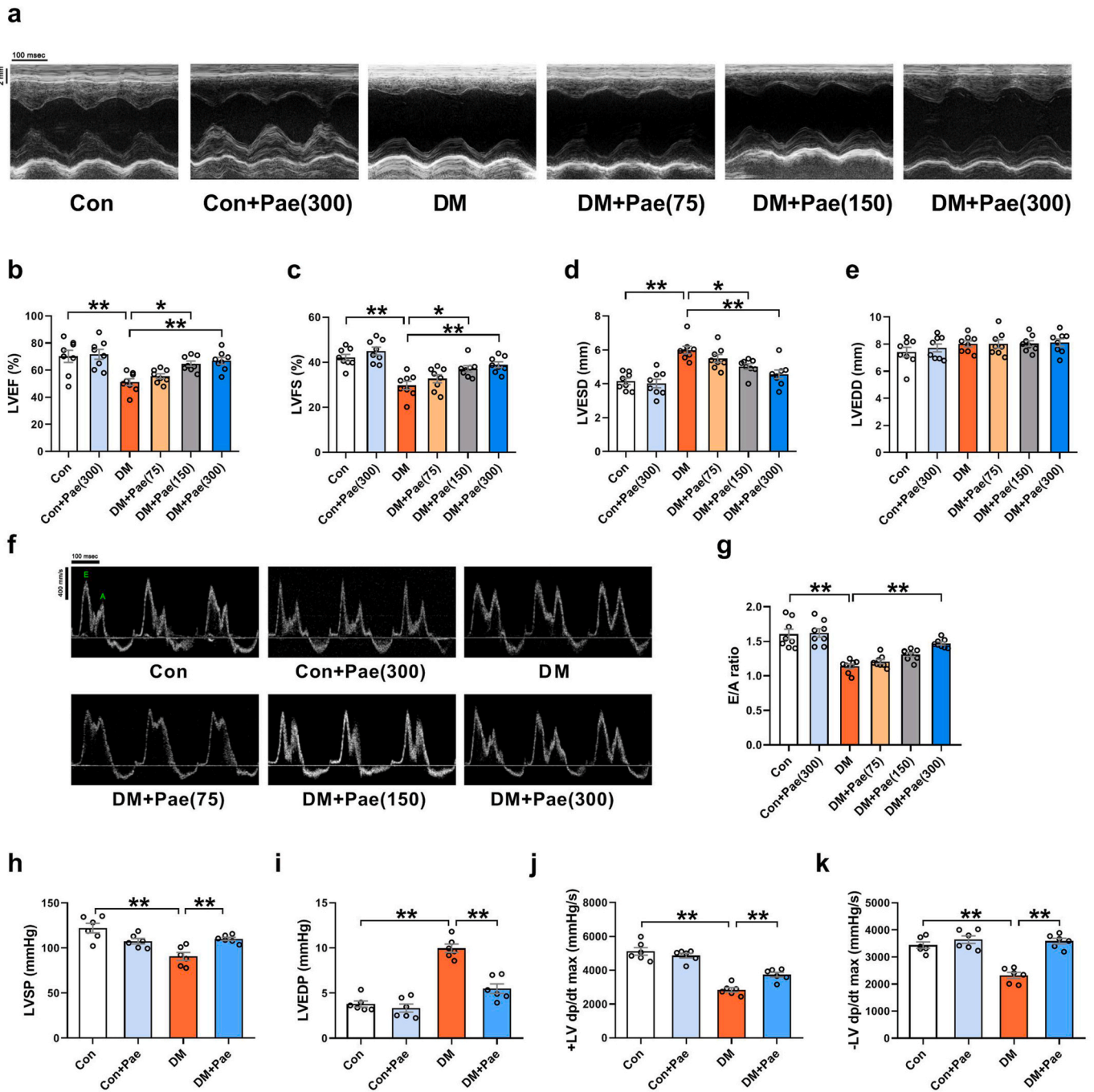


Fig. 3. Pae attenuated diabetes-induced cardiac functional abnormalities in rats. Control non-diabetic or diabetic rats were treated with Pae for 12 weeks and their cardiac function was analyzed. (a) Representative echocardiography images. (b-e) Quantitative analysis of echocardiography data including left ventricular ejection fraction (LVEF), left ventricular fractional shortening (LVFS), left ventricular end-systolic diameter (LVESD) and Left ventricular end-diastolic diameter (LVEDD). (f-g) Representative pulse-wave Doppler images and quantitative analysis of the E/A ratio. DM, diabetes mellitus; Pae (75, 150, 300), paeonol at a dosage of 75, 150 or 300 mg/kg/day respectively; $n = 8$ in each group. (h-k) Quantitative analysis of hemodynamic data including LV systolic pressure (LVSP), LV end-diastolic pressure (LVEDP) and the maximal and minimal first derivative of LV pressure (\pm LV dp/dtmax). Pae, paeonol at a dosage of 300 mg/kg/day; $n = 6$ in each group. All data are shown as means \pm SEM. * $P < 0.05$, ** $P < 0.01$.

3.5. Knockdown of *Opa1* with AAV-*Opa1* shRNA blunted the protective effects of Pae in diabetic hearts

To explore whether *Opa1* is essential for the cardiac protective effects of Pae *in vivo*, adeno-associated virus 9-harboring *Opa1* miRNA backbone-based shRNA (AAV-*Opa1* shRNA) construct was used to knockdown *Opa1* in the diabetic hearts. Since virus transfection efficiency is relatively low in rat hearts, mouse hearts were then used for

Opa1 gene silencing experiments. As shown in Fig. 6a, AAV-*Opa1* shRNA significantly reduced *Opa1* protein expression by $\sim 70\%$ in the diabetic hearts. Pae improved diastolic function as evidenced by the increased E/A ratio in the diabetic hearts receiving control shRNA (Fig. 6b and c). Moreover, Pae increased LVEF, decreased LVESD, inhibited myocardial oxidative stress and suppressed apoptosis in the diabetic hearts receiving Control shRNA (Fig. 6d-i), whereas all the effects were blunted in *Opa1* knockdown hearts (Fig. 6b-i). Pae

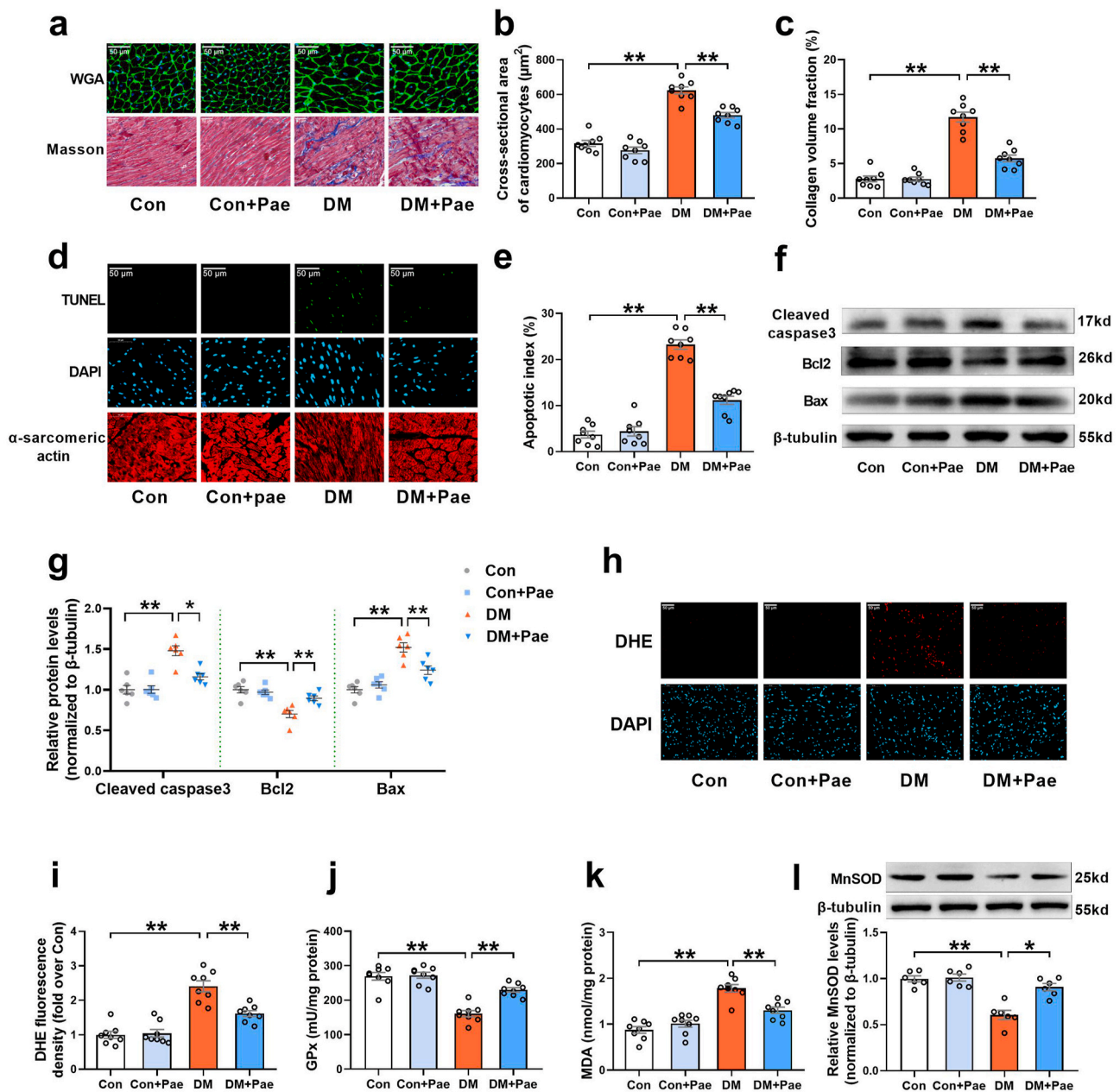


Fig. 4. Pae alleviated cardiac structural abnormalities and inhibited cardiomyocyte apoptosis and oxidative stress in diabetic hearts. **(a)** Representative images of cardiomyocyte size and interstitial fibrosis obtained using wheat germ agglutinin (WGA) staining and Masson trichrome staining respectively. Original magnification $\times 400$. **(b)** Quantification of average cross-sectional area of cardiomyocytes. **(c)** Interstitial fibrosis was quantified as collagen volume fraction. **(d)** Representative images of TUNEL and DAPI staining of heart tissues. Original magnification $\times 800$. **(e)** Percentage of apoptotic cells quantified as apoptotic index. **(f, g)** Representative blots and quantitative analysis of cleaved caspase 3, Bcl2, Bax and β -tubulin. **(h-i)** Representative images and quantitative analysis of DHE-stained heart tissues. Original magnification $\times 800$. **(j)** Glutathione peroxidase (GPx) activity. **(k)** Malondialdehyde (MDA) content. **(l)** Representative blots and quantitative analysis of Mitochondrial manganese superoxide dismutase (MnSOD). DM, diabetes mellitus; Pae, paeonol at a dosage of 300 mg/kg/day. $n = 8$ for animal experiments (Figure a–e, h–k) and $n = 6$ for Western blot experiments (Figure f–g, l). All data are shown as means \pm SEM. * $P < 0.05$, ** $P < 0.01$.

promoted mitochondrial fusion and increased cristae density in the diabetic hearts receiving control shRNA, as reflected by the reduced percentage of mitochondria with sizes $< 0.6 \mu\text{m}^2$, elevated percentage of mitochondria with sizes of $0.6\text{--}1 \mu\text{m}^2$ or $> 1 \mu\text{m}^2$, larger mean mitochondrial size and increased amount of cristae per mitochondrial area (Fig. 6j–o). Knockdown of Opa1 in the diabetic hearts largely abrogated the promoting effects of Pae on mitochondrial fusion and cristae density (Fig. 6j–o). These results indicated that Pae exerted its cardiac protective effects mainly via an Opa1-dependent way in the diabetic hearts.

3.6. Pae upregulated the expression of Opa1 via Stat3-mediated transcription

Li et al. has shown that Pae activates the PI3K signaling pathway in diabetic hearts [29]. To identify the signaling pathway that mediates the Pae-induced upregulation of Opa1, several specific inhibitors including wortmannin (Wort, a PI3K inhibitor) were used to screen for potential signaling pathways. As shown in Fig. 7a, the cardiomyocytes in the HG + Pae group were pretreated with the following agents: pyrrolidine dithiocarbamate (PDT, an NF- κ B inhibitor, 100 $\mu\text{mol/L}$, MedChem Express) [30], wortmannin (Wort, 0.1 $\mu\text{mol/L}$, MedChem Express) [31,

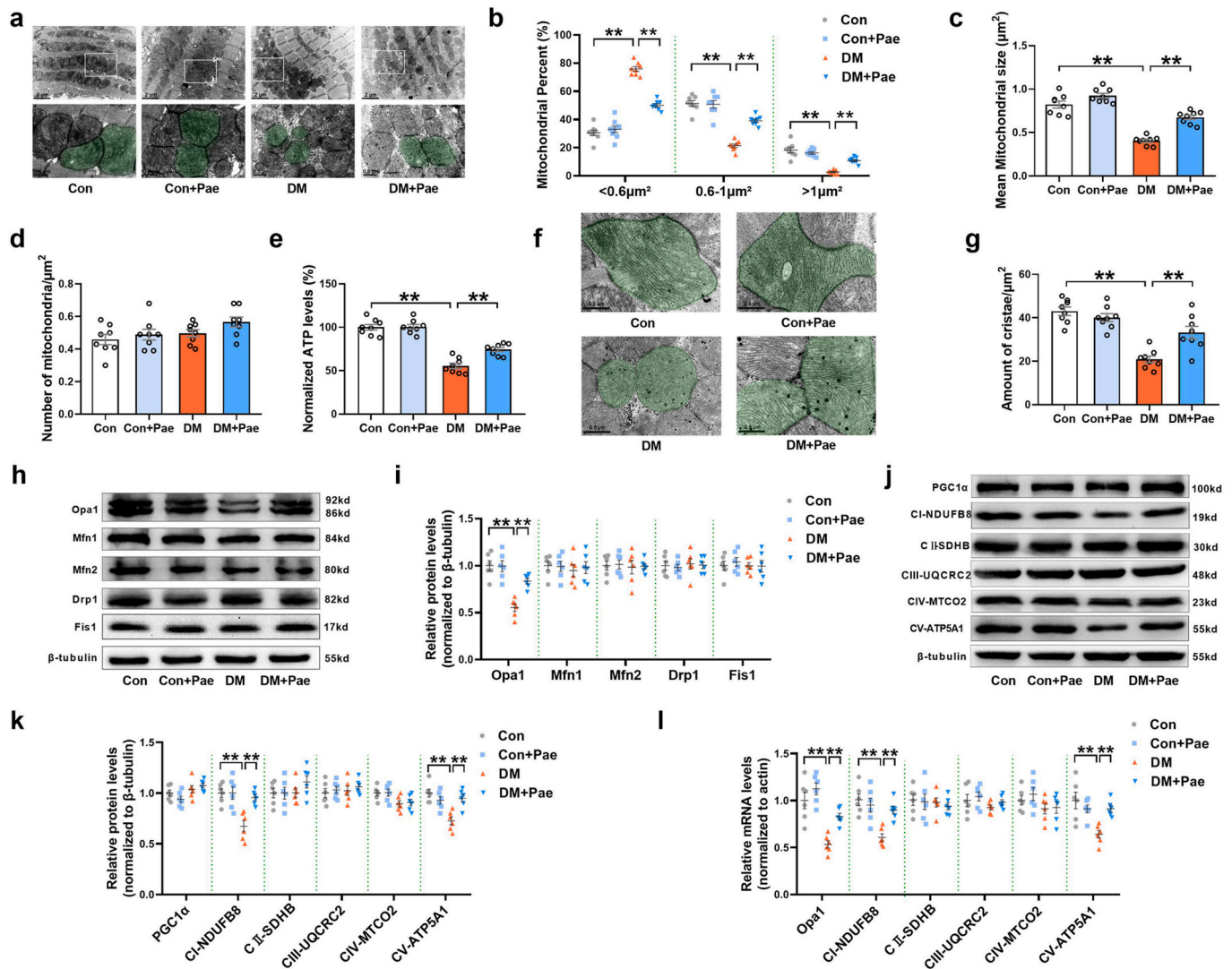


Fig. 5. Pae promoted Opa1-related mitochondrial fusion and restored mitochondrial function in diabetic hearts. (a) Representative images of mitochondrial morphology obtained by transmission electron microscope. Mitochondria are shown in green. Scale bars = 1 μm. Original magnification × 15,000. (b) Mitochondria were classified into three categories based on size (<0.6 μm², 0.6–1 μm², >1 μm²). (c) Quantification of mean mitochondrial size. (d) Quantification of mitochondrial number per μm². (e) Quantification of normalized ATP levels. (f) Representative images of mitochondrial cristae obtained by transmission electron microscope. Mitochondria are shown in green. Scale bars = 0.5 μm. Original magnification × 40,000. (g) Quantification of cristae amount per mitochondrial area. (h–i) Representative blots and quantitative analysis of mitochondrial fission/fusion-related proteins including Opa1, Mfn1, Mfn2, Drp1 and Fis1. (j–k) Representative blots and quantitative analysis of PGC-1α and mitochondrial respiratory chain complex I–V (CI–V). (l) Quantitative analysis of Opa1 and CI–V mRNA expression determined by real-time PCR. DM, diabetes mellitus; Pae, paeonol at a dosage of 300 mg/kg/day. n = 8 for animal experiments (Figure a–g) and n = 6 for molecular biology experiments (Figure h–l). All data are shown as means ± SEM. **P < 0.01. (For interpretation of the references to colour in this figure legend, the reader is referred to the Web version of this article.)

32], Stattic (a Stat3 inhibitor, 10 μmol/L, MedChem Express) [33,34], PD98059 (a MEK inhibitor, 20 μmol/L, MedChem Express) [35], and bisindolylmaleimide I (Bis, a PKC inhibitor, 10 μmol/L, MedChem Express) [36,37]. None of these inhibitors affected the expression of Opa1 in the HG-cultured cardiomyocytes in the absence of Pae (Supplementary Fig. S3). Pae-induced upregulation of Opa1 in the HG-cultured cardiomyocytes was largely blunted by Stattic pretreatment, whereas it was unaffected by the other inhibitors, indicating that the activation of Stat3 may be involved in the upregulation of Opa1 expression induced by Pae.

SiRNA was used to further explore whether Stat3 was responsible for regulating Opa1-mediated mitochondrial fusion in response to Pae treatment. As shown in Fig. 7b–f, knockdown of Stat3 by siRNA blocked the upregulating effects of Pae on phosphorylated Stat3 (p-Stat3 Tyr705, an active form of Stat3), total Stat3, Opa1 protein and mRNA, implying that Stat3 modulates the expression of Opa1 at the level of transcription.

Moreover, Stat3 siRNA blunted the promoting effects of Pae on mitochondrial fusion (Fig. 7g–i) and largely abrogated the inhibitory effects of Pae on mitochondrial oxidative stress (Fig. 7j). ChIP-PCR analysis revealed that Stat3 directly bound to the promoter of Opa1, while the binding was significantly decreased under HG conditions. Pae treatment significantly restored the binding of Stat3 to the Opa1 promoter in HG-treated cardiomyocytes (Fig. 7k). These data suggest that Pae promoted Opa1-mediated mitochondrial fusion and inhibited mitochondrial oxidative stress mainly in a Stat3-dependent transcriptional manner.

3.7. Pae increased Stat3 phosphorylation and promoted Opa1-mediated mitochondrial fusion via the CK2α-Jak2 signaling pathway

Pae is a highly liposoluble compound with a low molecular weight, which facilitates its easy transportation to the brain [38]. It is speculated that Pae can traverse the cell membrane and exert direct action on some

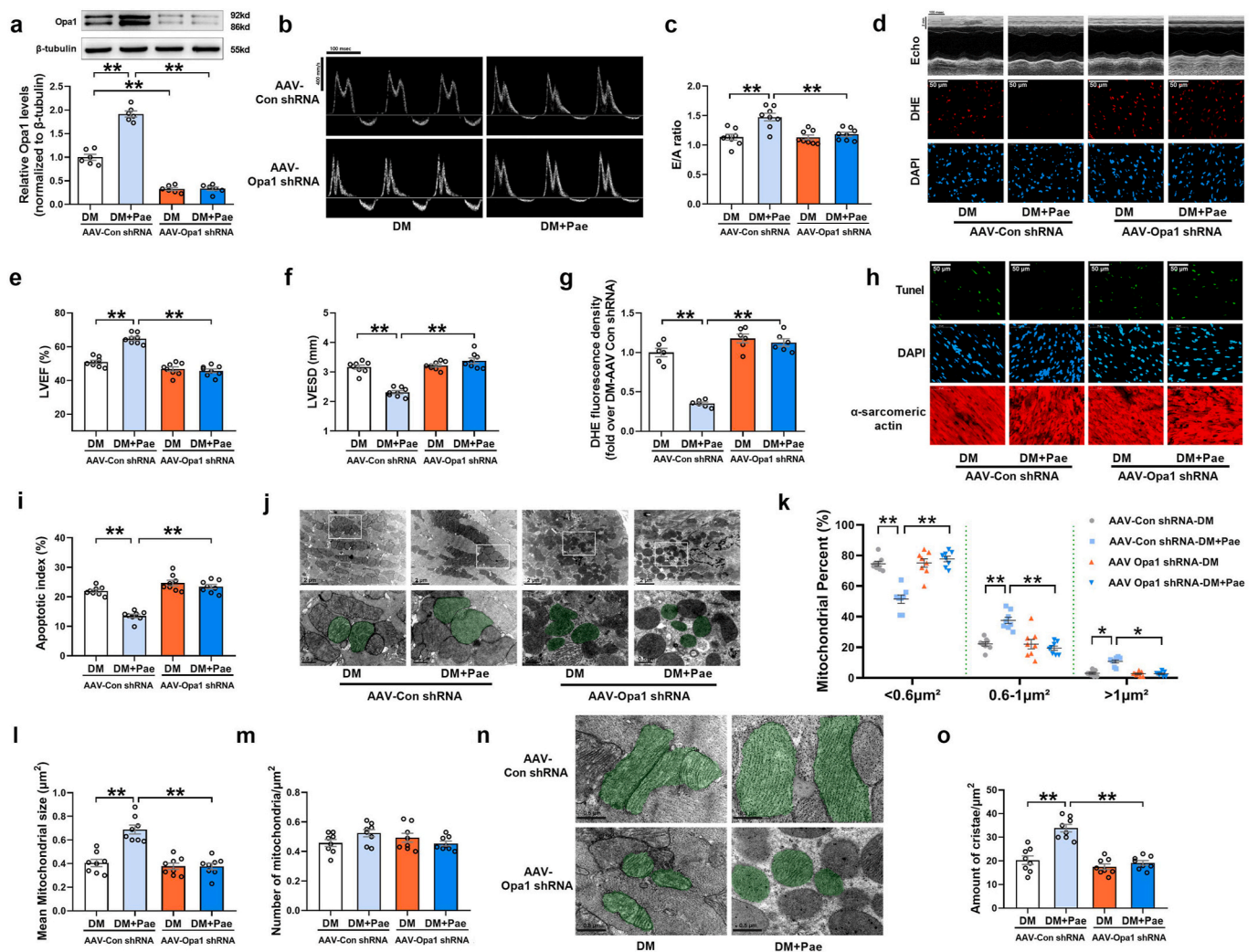


Fig. 6. Knockdown of Opa1 with AAV-Opa1 shRNA blunted the cardioprotective effects of Pae in diabetic hearts. (a) Representative blots and quantitative analysis of Opa1 expression. (b-c) Representative pulse-wave Doppler images and quantitative analysis of the E/A ratio. (d) Upper: Representative echocardiography images. Bottom: Representative images of DHE-stained heart tissues. Original magnification $\times 800$. (e-f) Quantitative analysis of echocardiography data including left ventricular ejection fraction (LVEF) and left ventricular end-systolic diameter (LVESD). (g) Quantitative analysis of DHE staining. (h) Representative images of TUNEL and DAPI staining of the heart tissues. Original magnification $\times 800$. (i) Percentage of apoptotic cells quantified as apoptotic index. (j) Representative images of mitochondrial morphology obtained by transmission electron microscope. Mitochondria are shown in green. Scale bars = 1 μm . Original magnification $\times 15,000$. (k) Mitochondria were classified into three categories based on their size (<0.6 μm^2 , 0.6–1 μm^2 , >1 μm^2). (l) Quantification of mean mitochondrial size. (m) Quantification of mitochondrial number per μm^2 . (n) Representative images of mitochondrial cristae obtained by transmission electron microscope. Mitochondria are shown in green. Scale bars = 0.5 μm . Original magnification $\times 40,000$. (o) Quantification of cristae amount per mitochondrial area. DM, diabetes mellitus; Pae, paeonol at a dosage of 300 mg/kg/day. n = 6 for Western blot and DHE experiments (Figure a, g) and n = 8 for animal experiments (Figure b–o). All data are shown as means \pm SEM. * $P < 0.05$, ** $P < 0.01$. (For interpretation of the references to colour in this figure legend, the reader is referred to the Web version of this article.)

adaptor molecules. To reveal the direct target of Pae, the SDF structure of Pae was submitted to the Pharammapper selecting “All Targets” Model, and the top 300 potential targets ranked by the normalized fit score in descending order were listed (job ID: 201215135510). The detailed results were uploaded as a separate file (Table 2). Since Stat3 phosphorylation is usually regulated by kinases, the function annotations containing “Involved in kinase activity” were selected and five candidates were identified, as seen in Fig. 8a, which were “Cell division protein kinase 2” (Rank 10), “Casein kinase II subunit alpha” (Rank 55), “Mitogen-activated protein kinase 14” (Rank 62), “Arginine kinase” (Rank 91) and “cAMP-dependent protein kinase catalytic subunit alpha” (Rank 233). According to the information provided by Universal Protein Resource (UniProt), cell division protein kinase 2 is involved in the control of the cell cycle; Mitogen-activated protein kinase 14 is one of the four p38 MAPKs which have been implicated in apoptosis induction; Arginine kinase catalyzes the reversible phosphorylation between

phosphoarginine and ADP. It seemed that the biological functions of these three kinases did not match the mitochondrial protective effects of Pae. Hence, CK2 α (casein kinase II subunit alpha) and PKA C α (cAMP-dependent protein kinase catalytic subunit alpha) were considered to be the most likely target candidates. A selective PKA inhibitor (PKA Inhibitor IV, 5 $\mu\text{mol/L}$, Santa Cruz) [39] and CK2 α inhibitor (TBB, 10 $\mu\text{mol/L}$, MedChem Express) [40] were then used to identify whether CK2 α or PKA C α was involved in the upregulation of Stat3 phosphorylation and Opa1 expression. As shown in Fig. 8b–e, the Pae-induced increase in Stat3 phosphorylation and Opa1 expression was blunted by TBB but not PKA inhibitor (PKAi), suggesting that CK2 α seemed to be the most likely target candidate of Pae in the activation of Stat3-Opa1 signaling.

The interaction between Pae and CK2 α was further explored using computation docking. The 2D and 3D structure of Pae were exhibited in Fig. 8f. The AutoDock Vina binding test indicated that Pae might

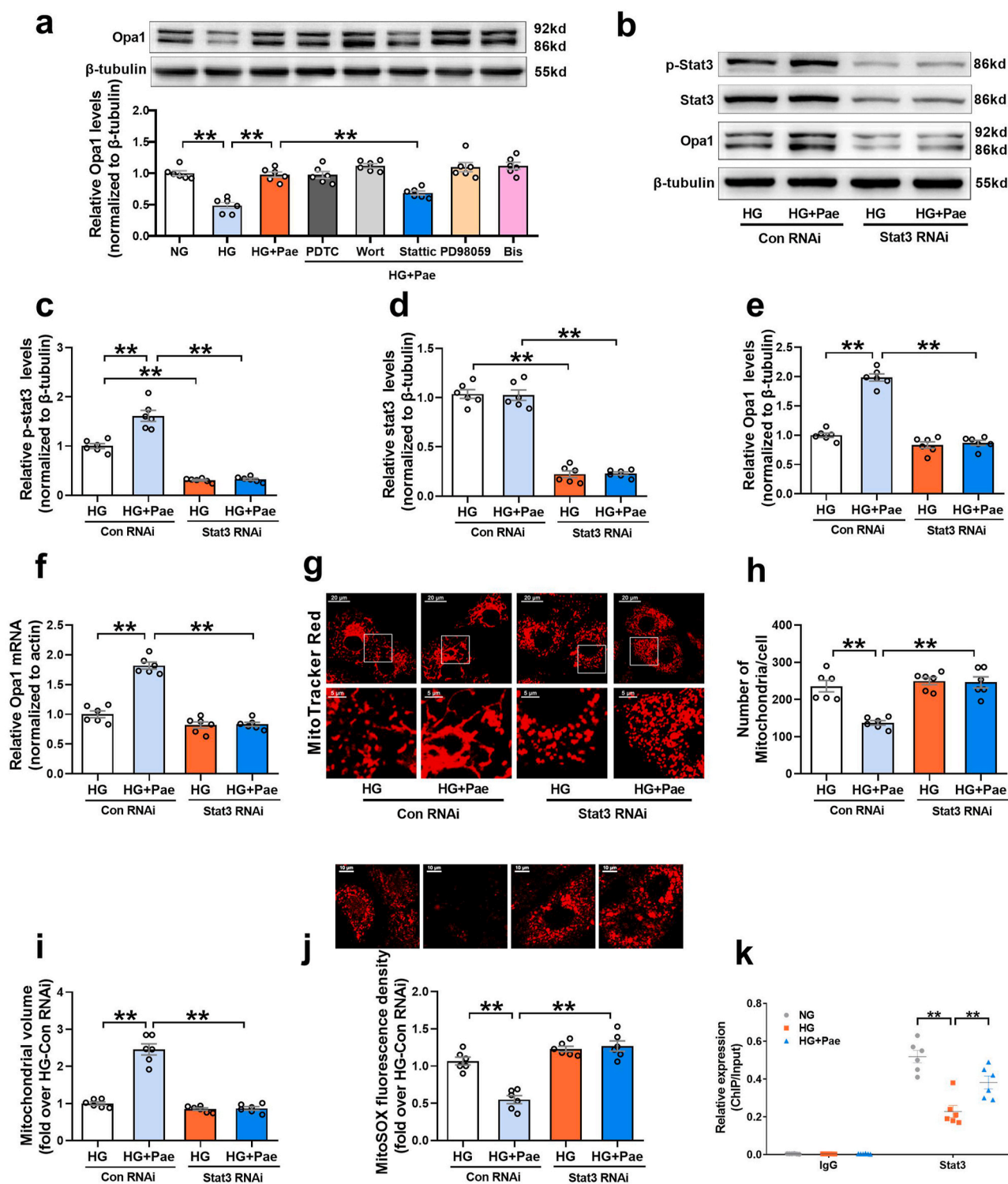


Fig. 7. Pae promoted Opa1-mediated mitochondrial fusion and inhibited mitochondrial oxidative stress in a Stat3-dependent way. (a) Several specific pharmacological inhibitors, including pyrrolidine dithiocarbamate (PDTC, an NF- κ B inhibitor), wortmannin (Wort, a PI3K inhibitor), Stattic (a Stat3 inhibitor), PD98059 (a MEK inhibitor) and bisindolylmaleimide I (Bis, a PKC inhibitor), were pre-administered to the cardiomyocytes in the HG + Pae group and then the expression of Opa1 was quantified. (b-f) Stat3 was knocked down by siRNA, after which the cells were subjected to high glucose (HG) with or without paeonol (Pae). The protein expression of phosphorylated Stat3 (p-Stat3), total Stat3 and Opa1 were quantified in (b-e). The mRNA expression of Opa1 was quantified in (f). (g) Representative confocal microscope images of mitochondrial morphology stained by MitoTracker Red. Original magnification $\times 600$. (h) Quantification of mitochondrial number per cell. (i) Quantification of mean mitochondrial volume. (j) Representative images and quantitative analysis of MitoSOX-stained mitochondria-derived superoxide production. (k) Chromatin immunoprecipitation (ChIP) and real-time PCR analysis for the binding of Stat3 to Opa1 promoter. $n = 6$ in each group. HG, high glucose (33 mmol/L); Pae, paeonol (100 μ mol/L). All data are shown as means \pm SEM. ** $P < 0.01$. (For interpretation of the references to colour in this figure legend, the reader is referred to the Web version of this article.)

Table 2
Top 300 potential targets of Pae predicted by PharmMapper.



Result of 201215135510
Top 300 targets ranked by normalized fit score in descending order
Paeonol.sdf - Paeonol

Ligand: 11092

Rank	PDB ID	Target Name	Number of Features	Fit Score	Normalized Fit Score	z'-score
1	1SV3	Phospholipase A2 VRV-PL-VIIIa	3	2.951	0.9838	1.87663
2	1OYB	NADPH dehydrogenase 1	3	2.921	0.9736	1.51791
3	1TG8	Genome polyprotein	3	2.844	0.9481	1.55992
4	1P01	Cholinesterase	3	2.827	0.9423	1.37953
5	1OGS	Glucosylceramidase	3	2.807	0.9356	1.32505
6	3MTH	Insulin	3	2.746	0.9155	0.969419
7	1JU3	Cocaine esterase	3	2.701	0.9004	0.943124

8	1UK7	NONE	3	2.652	0.884	0.516397
9	1VXR	Acetylcholinesterase	3	2.62	0.8734	0.610523
10	2VTA	Cell division protein kinase 2	3	2.42	0.8066	0.0149787
11	3BLS	Beta-lactamase	3	2.377	0.7925	-0.590482
12	1D0D	P-hydroxybenzoate hydroxylase	5	3.874	0.7748	5.76014
13	1OJA	Amine oxidase [flavin-containing] B	3	2.323	0.7742	-0.304784
14	1A8U	Non-heme chloroperoxidase	3	2.294	0.7646	-0.582959
15	1FP1	Isoliquiritigenin 2-O-methyltransferase	5	3.794	0.7588	5.83131
16	1VOH	Ascorbate peroxidase	4	2.953	0.7382	1.90625
17	1KTA	Branched-chain-amino-acid aminotransferase, mitochondrial	4	2.943	0.7357	1.64141
18	1HJG	Deacetoxycephalosporin C synthetase	4	2.927	0.7318	1.54431
19	1K2I	Chymotrypsinogen A	4	2.918	0.7294	1.62066
20	1G67	Thiamine-phosphate pyrophosphorylase	4	2.906	0.7265	1.49931
21	1MFU	Alpha-amylase 1	4	2.893	0.7233	1.64252
22	1CTU	Cytidine deaminase	4	2.872	0.7179	1.50962

23	LJGS	Multiple antibiotic resistance protein marR	4	2.862	0.7156	1.08388
24	IGIQ	P-selectin	3	2.145	0.7149	-1.43601
25	ITJY	Autoinducer 2-binding protein lsrB	4	2.823	0.7057	1.35346
26	ICW4	Isocitrate dehydrogenase [NADP]	4	2.82	0.705	1.05142
27	LNHB	Lysozyme	4	2.81	0.7025	1.15777
28	LLCP	Cytosol aminopeptidase	4	2.807	0.7018	1.1456
29	IH7O	Delta-aminolevulinic acid dehydratase	4	2.807	0.7018	1.22158
30	3PAX	Poly [ADP-ribose] polymerase 1	4	2.795	0.6988	1.06118
31	IQFL	Acetyl-CoA acetyltransferase	4	2.775	0.6938	1.14047
32	IQIQ	Isopenicillin N synthetase	4	2.765	0.6912	1.09023
33	LL1R	Adenine phosphoribosyltransferase	4	2.758	0.6896	0.892477
34	IC5O	Prothrombin	4	2.757	0.6894	0.996531
35	ILLUO	Trypsin inhibitor 1	4	2.75	0.6875	0.919321
36	ICS1	Cystathionine gamma-synthase	4	2.738	0.6845	0.715759
37	IK59	Angiogenin	4	2.718	0.6796	0.623112

38	1D1C	Complement factor D	4	2.714	0.6785	0.774422
39	1XIY	Peroxiredoxin	4	2.706	0.6765	0.325921
40	1QH9	(S)-2-haloacid dehalogenase	4	2.699	0.6748	0.475916
41	1SD1	UPF0274 protein ycfC	4	2.698	0.6745	0.712246
42	1U1W	Phenazine biosynthesis protein phzF	4	2.677	0.6692	0.579797
43	1F07	5,10-methylenetetrahydromethanopterin reductase	4	2.668	0.667	0.715004
44	1F4N	Regulatory protein rop	4	2.656	0.6641	0.574902
45	1FKW	Adenosine deaminase	4	2.655	0.6636	0.619741
46	1T6C	Exopolyphosphatase	4	2.649	0.6622	0.494787
47	1GJM	Camphor 5-monooxygenase	4	2.64	0.66	0.293797
48	1L9W	3-dehydroquininate dehydratase	4	2.629	0.6573	0.141873
49	2FUS	Fumarate hydratase class II	4	2.609	0.6522	0.332249
50	1M7P	Triosephosphate isomerase	4	2.597	0.6491	-0.0243719
51	1I4U	Crustacyanin-C1 subunit	4	2.575	0.6438	0.219021
52	2SN3	Toxin CsEv3	4	2.561	0.6401	0.176877

53	1CZC	Aspartate aminotransferase	4	2.547	0.6368	-0.213528
54	1R16	ADP-ribosyl cyclase	4	2.544	0.6361	-0.0302488
55	1M2P	Casein kinase II subunit alpha	4	2.54	0.6351	0.119779
56	1M9J	Nitric oxide synthase, endothelial	4	2.486	0.6216	-0.37268
57	1F3X	Pyruvate kinase isozymes M1/M2	4	2.423	0.6057	-1.09924
58	1FMS	Chalcone--flavonone isomerase 1	5	2.973	0.5946	1.8216
59	1N5V	ActVA 6 protein	5	2.963	0.5927	1.67939
60	1TTJ	Triosephosphate isomerase, glycosomal	5	2.96	0.592	1.41171
61	3EKR	Heat shock protein HSP 90-alpha	5	2.95	0.59	1.65513
62	1DI9	Mitogen-activated protein kinase 14	5	2.94	0.5881	1.38111
63	1UWS	Beta-galactosidase	5	2.935	0.5871	1.356
64	1PDZ	Enolase	5	2.929	0.5859	1.1247
65	1X92	Phosphoheptose isomerase	5	2.929	0.5857	1.75824
66	1WD1	S-adenosylmethionin	5	2.924	0.5847	1.61819
67	1S89	Methylglyoxal synthase	5	2.919	0.5838	1.20805

68	2C3L	Serine/threonine-protein kinase Chk1	4	2.335	0.5838	-0.85528
69	1.00E+90	Phosphatidylinositol-4,5-bisphosphate 3-kinase catalytic subunit gamma isoform	5	2.914	0.5827	1.79326
70	1CK6	Peroxidase	5	2.913	0.5826	1.57109
71	1GPY	Glycogen phosphorylase, muscle form	5	2.912	0.5824	1.38803
72	2VKU	Cytochrome P450 51	5	2.912	0.5824	1.34259
73	1GT7	Rhamnulose-1-phosphate aldolase	5	2.891	0.5783	1.34424
74	1X02	Cell division protein kinase 6	5	2.883	0.5765	1.33332
75	1Q41	Glycogen synthase kinase-3 beta	5	2.877	0.5754	1.44772
76	1VJ5	Epoxide hydrolase 2	5	2.872	0.5743	1.01679
77	1LQP	Glutathione transferase fosA	5	2.871	0.5741	0.804652
78	3FZL	Heat shock cognate 71 kDa protein	5	2.865	0.5729	1.57221
79	1UAE	UDP-N-acetylglucosamine 1-carboxyvinyltransferase	5	2.864	0.5727	0.811521
80	5PTP	Cationic trypsin	5	2.847	0.5694	1.45835
81	1AGW	Basic fibroblast growth factor receptor 1	4	2.275	0.5687	-1.07475
82	1TLZ	Nucleoside-specific channel-forming protein tsx precursor	4	2.271	0.5679	-1.12861

83	1TLS	Thymidylate synthase	5	2.83	0.5659	1.17947
84	1GP5	Leucoanthocyanidin dioxygenase	5	2.815	0.5631	0.810429
85	1A7A	Adenosylhomocysteinase	5	2.808	0.5617	0.7841
86	1HXP	Galactose-1-phosphate uridylyltransferase	5	2.808	0.5617	0.965529
87	1MOY	Streptavidin	5	2.793	0.5587	0.976807
88	1R10	Arginase-1	5	2.791	0.5582	0.821209
89	2H0H	Guanyl-specific ribonuclease T1	5	2.789	0.5578	1.18543
90	1W55	Bifunctional enzyme ispD/ispF	5	2.781	0.5561	0.493262
91	1BG0	Arginine kinase	5	2.777	0.5555	0.93766
92	1M3U	3-methyl-2-oxobutanoate hydroxymethyltransferase	5	2.758	0.5515	0.617323
93	1DJP	Glutaminase-asparaginase	5	2.749	0.5498	0.985547
94	1S50	Glutamate receptor, ionotropic kainate 2	5	2.748	0.5496	0.42112
95	1F92	Urokinase-type plasminogen activator	5	2.747	0.5494	0.933523
96	1CNW	Carbonic anhydrase 2	5	2.745	0.549	0.444343
97	1YW1	Putative monooxygenase moxC	5	2.745	0.5489	0.442319

98	1KSV	Ribosomal small subunit pseudouridine synthase A	5	2.726	0.5453	0.71733
99	1K7T	Agglutinin isolectin 3	5	2.72	0.5441	0.64175
100	1DUV	Ornithine carbamoyltransferase chain I	5	2.72	0.5439	0.289159
101	1HK8	Anaerobic ribonucleoside-triphosphate reductase	5	2.717	0.5434	-0.105949
102	1WLJ	Interferon-stimulated gene 20 kDa protein	5	2.717	0.5434	0.167062
103	1MX9	Liver carboxylesterase I	5	2.715	0.543	0.783333
104	1E2J	Thymidine kinase	5	2.695	0.539	0.546648
105	1J2R	Isochorismatase family protein yecD	5	2.692	0.5384	0.307833
106	1S2P	Crustacyanin-A1 subunit	5	2.69	0.538	0.346903
107	1JPC	Mannose-specific lectin	5	2.68	0.536	0.0874683
108	1XMC	Peroxisomal carnitine 0-octanoyltransferase	5	2.673	0.5346	0.339238
109	2DIJ	Cyclomaltodextrin glucanotransferase	5	2.668	0.5336	0.577768
110	1C7Z	6-phosphofructo-2-kinase/fructose-2,6-biphosphatase 1	5	2.659	0.5317	-0.224843
111	1MDR	Mandelate racemase	5	2.648	0.5296	-0.0769986
112	1VKE	Hypothetical protein	5	2.637	0.5273	0.0972302

113	1MM6	Glutamate receptor 2	5	2.633	0.5266	0.204647
114	2CHT	Chorismate mutase	5	2.627	0.5254	-0.170334
115	1MN1	Peroxidase manganese-dependent 1	5	2.625	0.5251	0.509059
116	2UZB	Cyclin-A2	5	2.619	0.5239	0.000909615
117	4FUA	L-fuculose phosphate aldolase	5	2.608	0.5217	-0.345969
118	1H6G	Catenin alpha-1	5	2.605	0.521	-0.00672488
119	1LRM	Phenylalanine-4-hydroxylase	5	2.592	0.5184	0.384849
120	1M6K	Beta-lactamase OXA-1	5	2.588	0.5176	-0.114472
121	1Y89	DevB protein	5	2.568	0.5135	0.276313
122	1PFW	Methionyl-tRNA synthetase	6	3.067	0.5112	1.5375
123	1DQY	Antigen 85-C	5	2.553	0.5107	-0.477554
124	1EQC	Glucan 1,3-beta-glucosidase	5	2.523	0.5045	-0.372156
125	1ADO	Fructose-bisphosphate aldolase A	5	2.517	0.5033	-0.999412
126	1IV2	2-C-methyl-D-erythritol 2,4-cyclodiphosphate synthase	5	2.508	0.5016	-0.296171
127	1EWK	Metabotropic glutamate receptor 1	5	2.502	0.5004	-0.474907

128	1QR7	Phospho-2-dehydro-3-deoxyheptonate aldolase, Phe-sensitive	5	2.501	0.5002	-0.787945
129	1BF6	Phosphotriesterase homology protein	5	2.493	0.4987	-0.416802
130	1117	DNA double-strand break repair protein mre11	6	2.979	0.4965	1.6061
131	1KMQ	Transforming protein RhoA	5	2.48	0.496	-0.225048
132	3B8R	Vascular endothelial growth factor receptor 2	5	2.475	0.495	-0.365955
133	1RMY	Class B acid phosphatase	5	2.47	0.4939	-0.448704
134	1X1L	Superoxide dismutase [Mn], mitochondrial	5	2.468	0.4937	-0.614834
135	1L5R	Glycogen phosphorylase, liver form	6	2.961	0.4935	1.28273
136	1OF8	Phospho-2-dehydro-3-deoxyheptonate aldolase, tyrosine-inhibited	6	2.96	0.4934	1.30287
137	1X7N	Glucose-6-phosphate isomerase	6	2.959	0.4932	0.956049
138	1XUZ	Capsule biosynthesis protein	6	2.951	0.4919	0.858512
139	1XLR	Chorismate--pyruvate lyase	5	2.457	0.4914	-0.786716
140	1NHX	Phosphoenolpyruvate carboxykinase, cytosolic [GTP]	6	2.947	0.4912	0.891791
141	1O4H	Proto-oncogene tyrosine-protein kinase Src	6	2.947	0.4911	0.69549
142	2BKL	Prolyl endopeptidase Pep	6	2.947	0.4911	0.465309

143	2RNF	Ribonuclease 4	5	2.455	0.4911	-0.715217
144	1EQJ	2,3-bisphosphoglycerate-independent phosphoglycerate mutase	6	2.946	0.491	0.713786
145	1H49	Beta-glucosidase, chloroplastic	6	2.946	0.491	1.77494
146	1PZM	Hypoxanthine-guanine phosphoribosyltransferase	5	2.453	0.4906	-1.22329
147	1DE5	L-rhamnose isomerase	6	2.942	0.4904	1.70568
148	1UF7	N-carbamoyl-D-amino acid hydrolase	6	2.935	0.4891	0.997292
149	1Q4W	Queuine tRNA-ribosyltransferase	5	2.435	0.4869	-0.844697
150	1QFS	Prolyl endopeptidase	6	2.918	0.4863	1.32036
151	1DQ8	3-hydroxy-3-methylglutaryl-coenzyme A reductase	5	2.427	0.4855	-1.07414
152	1DAM	Dethiobiotin synthetase	6	2.911	0.4851	0.547106
153	1WD4	Alpha-N-arabinofuranosidase B	6	2.907	0.4845	1.54631
154	1S2C	Aldo-keto reductase family 1 member C3	6	2.907	0.4845	1.1046
155	1S17	Peptide deformylase	6	2.907	0.4845	1.04261
156	1DRY	Clavamate synthase 1	6	2.9	0.4834	0.913348
157	1H1H	Eosinophil cationic protein	6	2.899	0.4831	1.14519

158	INQA	Glyceraldehyde-3-phosphate dehydrogenase	6	2.898	0.4829	0.400502
159	IM4B	Interleukin-2	6	2.897	0.4828	1.43549
160	INY0	Beta-lactamase TEM	6	2.896	0.4827	1.41685
161	IX98	Aldose reductase	6	2.893	0.4821	0.946905
162	IKPH	Cyclopropane-fatty-acyl-phospholipid synthase 1	6	2.89	0.4817	0.571183
163	ISEH	Deoxyuridine 5-triphosphate nucleotidohydrolase	6	2.887	0.4811	0.29448
164	IOG5	Cytochrome P450 2C9	6	2.878	0.4796	0.919256
165	IKWU	Mannose-binding protein A	6	2.873	0.4788	0.720406
166	IFWT	2-dehydro-3-deoxyphosphooctonate aldolase	6	2.866	0.4776	0.60674
167	IKF0	Phosphoglycerate kinase 1	6	2.865	0.4775	0.403939
168	IP48	Enolase 1	6	2.864	0.4774	0.471329
169	IWDS	Beta-amylase	6	2.861	0.4768	0.736727
170	IROB	Ribonuclease pancreatic	6	2.854	0.4756	0.34807
171	2GGB	Methionine aminopeptidase	6	2.846	0.4743	1.41785
172	IF06	Meso-diaminopimelate D-dehydrogenase	6	2.845	0.4742	0.928829

173	1DR1	Dihydrofolate reductase	6	2.845	0.4742	1.3273
174	1S8G	Phospholipase A2 homolog MT1	6	2.835	0.4724	0.253214
175	1LP6	Orotidine 5-phosphate decarboxylase	6	2.834	0.4724	0.965394
176	1QMG	Ketol-acid reductoisomerase, chloroplast	6	2.832	0.4721	0.928577
177	1RJ4	Invertase inhibitor	6	2.832	0.4719	1.221
178	1U8X	Maltose-6-phosphate glucosidase	5	2.36	0.4719	-1.0479
179	1MZ6	Sialidase	5	2.357	0.4715	-1.60329
180	1IXN	Pyridoxine 5-phosphate synthase	7	3.299	0.4712	1.90601
181	1A9P	Purine nucleoside phosphorylase	6	2.817	0.4695	1.1655
182	1N94	Protein farnesyltransferase/geranylgeranyltransferase type-1 subunit alpha	6	2.816	0.4693	0.551408
183	2QCF	Uridine 5-monophosphate synthase	6	2.805	0.4675	0.939935
184	5TLN	Thermolysin	6	2.799	0.4665	0.863039
185	1A2Q	Subtilisin BPN	6	2.799	0.4665	0.356017
186	1FR8	Beta-1,4-galactosyltransferase 1	6	2.787	0.4646	0.939798
187	1U4L	C-C motif chemokine 5	6	2.784	0.464	0.943774

188	1UMZ	Xyloglucan endotransglycosylase	5	2.32	0.464	-1.29686
189	1ATL	Zinc metalloproteinase atrolysin-D	6	2.775	0.4625	0.469595
190	1NE4	cAMP-dependent protein kinase type I-alpha regulatory subunit	6	2.771	0.4618	0.415469
191	1JSR	L-asparaginase	5	2.295	0.459	-1.14128
192	1RFJ	Calmodulin-5/6/7/8	6	2.752	0.4587	0.141916
193	1TKU	3,4-dihydroxy-2-butanone 4-phosphate synthase	6	2.75	0.4584	-0.0957835
194	1GWW	N-acetyllactosaminide alpha-1,3-galactosyltransferase	6	2.741	0.4568	0.515092
195	1YWQ	Nitroreductase family protein	6	2.733	0.4555	0.624144
196	1J01	Neopullulanase	6	2.727	0.4545	0.931219
197	1MD2	Cholera enterotoxin subunit B	6	2.722	0.4537	0.487317
198	1QZ6	Actin, alpha skeletal muscle	6	2.719	0.4531	0.396327
199	1VBO	Mannose-specific lectin KM+	6	2.711	0.4518	0.209182
200	1R6Z	Maltose-binding periplasmic protein	6	2.705	0.4509	0.352641
201	1Y2D	cAMP-specific 3,5-cyclic phosphodiesterase 4D	6	2.689	0.4482	-0.19357
202	1FK1	Nonspecific lipid-transfer protein	6	2.68	0.4466	-0.335506

203	1V9L	Glutamate dehydrogenase	5	2.227	0.4454	-1.30416
204	1ACM	Aspartate carbamoyltransferase catalytic chain	6	2.67	0.4451	0.0590876
205	1AHP	Maltodextrin phosphorylase	6	2.661	0.4435	0.358467
206	1W2G	Thymidylate kinase	5	2.207	0.4414	-2.09933
207	1Y9Q	Transcriptional regulator, HTH_3 family	6	2.629	0.4382	-0.0711819
208	1JH7	Cyclic phosphodiesterase	6	2.618	0.4364	-0.228552
209	1ISG	ADP-ribosyl cyclase 2	6	2.609	0.4349	-0.347577
210	1SJD	N-acylamino acid racemase	6	2.606	0.4343	-0.226936
211	1RXU	Uridine phosphorylase	6	2.598	0.4331	0.0144487
212	1J20	Argininosuccinate synthase	6	2.598	0.433	-0.117796
213	1GTK	Porphobilinogen deaminase	5	2.164	0.4328	-1.69586
214	6PFK	6-phosphofructokinase	6	2.593	0.4322	-0.541464
215	1KNM	Endo-1,4-beta-xylanase A	6	2.592	0.432	0.192925
216	1CY1	DNA topoisomerase 1	5	2.159	0.4317	-2.32672
217	1C41	6,7-dimethyl-8-ribityllumazine synthase	6	2.583	0.4304	-0.197995

218	1WRR	Uricase	6	2.581	0.4302	0.128908
219	1JCJ	Deoxyribose-phosphate aldolase	6	2.577	0.4296	-0.539714
220	2GBP	D-galactose-binding periplasmic protein precursor	6	2.554	0.4257	-0.71278
221	2BET	Ribose-5-phosphate isomerase B	8	3.405	0.4256	2.06758
222	1NGS	Transketolase 1	6	2.552	0.4253	-0.411867
223	1RQ2	Cell division protein ftsZ	6	2.546	0.4243	-0.59242
224	1QW8	Alpha-N-arabinofuranosidase	7	2.956	0.4223	1.17297
225	1X9I	Bifunctional phosphoglucose/phosphomannose isomerase	7	2.952	0.4217	1.01429
226	1U11	N5-carboxyaminoimidazole ribonucleotide mutase	6	2.53	0.4217	-0.702669
227	1M09	2-oxopropyl-CoM reductase, carboxylating	5	2.107	0.4214	-2.75414
228	1QWN	Alpha-mannosidase 2	6	2.527	0.4211	-0.513941
229	1M0S	Ribose-5-phosphate isomerase A	6	2.526	0.421	-0.839753
230	1JEO	3-hexulose-6-phosphate isomerase	6	2.525	0.4208	-0.920089
231	1CW2	Tryptophan synthase alpha chain	7	2.945	0.4207	0.907163
232	1070	Fasciclin-1	7	2.936	0.4194	1.08623

233	20H0	cAMP-dependent protein kinase catalytic subunit alpha	6	2.515	0.4192	-0.0107484
234	1H72	Homoserine kinase	11	4.603	0.4185	1.01378
235	1NR5	Pentafunctional AROM polypeptide	7	2.927	0.4181	1.10682
236	1G0H	Inositol-1-monophosphatase	6	2.509	0.4181	-1.09146
237	1FPU	Proto-oncogene tyrosine-protein kinase ABL1	7	2.922	0.4175	0.274756
238	1BR5	Ricin	7	2.921	0.4173	1.67743
239	1NC3	5-methylthioadenosine/S-adenosylhomocysteine nucleosidase	7	2.921	0.4173	1.05098
240	1LJR	Glutathione S-transferase theta-2	7	2.92	0.4172	1.01024
241	1TE2	Phosphatase yniC	5	2.086	0.4172	-2.5747
242	2UZV	cAMP-dependent protein kinase inhibitor alpha	6	2.499	0.4166	-0.103999
243	1Z57	Dual specificity protein kinase CLK1	7	2.915	0.4164	1.22157
244	1ICQ	12-oxophytodienoate reductase 1	7	2.913	0.4162	0.370187
245	1HZE	Riboflavin synthase alpha chain	6	2.497	0.4162	-0.656058
246	1TIS	1-deoxy-D-xylulose 5-phosphate reductoisomerase	7	2.909	0.4156	0.543226
247	7CEL	Exoglucanase 1	7	2.905	0.415	1.11334

248	1RMO	Inositol-3-phosphate synthase	7	2.903	0.4147	0.96633
249	1QDQ	Cathepsin B	7	2.903	0.4146	1.07808
250	1P62	Deoxycytidine kinase	7	2.902	0.4146	1.02593
251	1PA9	Tyrosine-protein phosphatase yopH	7	2.898	0.414	0.692564
252	1UWJ	B-Raf proto-oncogene serine/threonine-protein kinase	7	2.894	0.4135	0.537533
253	1DQQ	Macrophage mannose receptor 1	7	2.893	0.4133	0.582708
254	1OVG	Purine nucleoside phosphorylase deoD-type	6	2.477	0.4128	-1.0602
255	1EEF	Heat-labile enterotoxin B chain	7	2.889	0.4127	1.10519
256	2W6P	Biotin carboxylase	7	2.879	0.4113	0.577867
257	1VAG	Nitric oxide synthase, brain	6	2.466	0.411	-0.942234
258	1C85	Tyrosine-protein phosphatase non-receptor type 1	7	2.876	0.4109	0.872761
259	1UCD	Ribonuclease MC	7	2.869	0.4098	0.750778
260	1P77	Shikimate dehydrogenase	7	2.868	0.4097	1.2252
261	1LWD	Isocitrate dehydrogenase [NADP], mitochondrial	7	2.867	0.4095	0.208181
262	1MOU	Glutathione S-transferase S1	7	2.863	0.409	0.913293

263	1BB7	Lysozyme C II	7	2.86	0.4086	0.815046
264	1MD0	UDP-4-amino-4-deoxy-L-arabinose--oxoglutarate aminotransferase	7	2.857	0.4081	0.75552
265	1V2A	Glutathione transferase gst1-6	7	2.851	0.4073	0.828823
266	1FHE	Glutathione S-transferase class-mu 26 kDa isozyme 47	6	2.444	0.4073	-0.760799
267	1GYM	1-phosphatidylinositol phosphodiesterase	7	2.85	0.4071	1.01241
268	1D8F	Stromelysin-1	7	2.839	0.4056	0.870434
269	7CPA	Carboxypeptidase A1	6	2.434	0.4056	-0.472248
270	1MLD	Malate dehydrogenase, mitochondrial	7	2.827	0.4039	0.396837
271	1Q6R	3-keto-L-gulonate-6-phosphate decarboxylase ulaD	6	2.422	0.4036	-1.36142
272	1L7P	Phosphoserine phosphatase	6	2.416	0.4027	-1.35955
273	1RZM	Phospho-2-dehydro-3-deoxyheptonate aldolase	5	2.01	0.402	-3.09141
274	1QZ3	Hydrolase	7	2.811	0.4015	0.194807
275	11H7	DNA polymerase	7	2.807	0.401	0.685222
276	1NQC	Cathepsin S	7	2.803	0.4004	0.539615
277	1X9D	Endoplasmic reticulum mannosyl-oligosaccharide 1,2-alpha-mannosidase	7	2.796	0.3995	0.733861

278	1UC2	UPF0027 protein PH1602	7	2.792	0.3989	1.12856
279	1O1X	Ras-related protein Rab-11A	6	2.393	0.3989	-0.996239
280	1E8V	Hemagglutinin-neuraminidase	7	2.779	0.397	0.343375
281	1P5G	Phosphomannomutase/phosphoglucomutase	7	2.778	0.3969	-0.0154689
282	1Z1D	Enoyl-[acyl-carrier-protein] reductase [NADH]	7	2.773	0.3961	1.02107
283	1H1B	Leukocyte elastase	6	2.372	0.3953	-1.3656
284	1BJ4	Serine hydroxymethyltransferase, cytosolic	6	2.371	0.3952	-0.893708
285	2BKX	Glucosamine-6-phosphate deaminase 1	7	2.763	0.3948	-0.0666402
286	1KL2	Serine hydroxymethyltransferase	6	2.366	0.3943	-1.1567
287	1LKX	Myosin IE heavy chain	7	2.756	0.3938	0.0107574
288	6FIT	Bis(5-adenosyl)-triphosphatase	6	2.357	0.3928	-1.01375
289	1M98	Orange carotenoid-binding protein	7	2.749	0.3927	0.650279
290	1YKD	Adenylate cyclase	7	2.747	0.3925	-0.0776722
291	1VLH	Phosphopantetheine adenylyltransferase	7	2.747	0.3924	-0.280405
292	1CKN	mRNA-capping enzyme	7	2.73	0.39	0.550394
293	1HV7	Chymotrypsin-like elastase family member 1	7	2.727	0.3896	0.354492
294	1XGE	Dihydroorotase	7	2.727	0.3895	0.0655277
295	1EGQ	Myrosinase MA1	7	2.726	0.3894	-0.041306
296	1RAO	2-amino-4-hydroxy-6-hydroxymethyl-dihydropteridine pyrophosphokinase	7	2.718	0.3883	-0.29314
297	1MI4	3-phosphoshikimate 1-carboxyvinyltransferase	7	2.718	0.3883	-0.0588795
298	1JHA	Nicotinate-nucleotide--dimethylbenzimidazole phosphoribosyltransferase	7	2.718	0.3883	-0.171737
299	3D2E	Heat shock protein homolog SSE1	6	2.33	0.3883	-1.31982

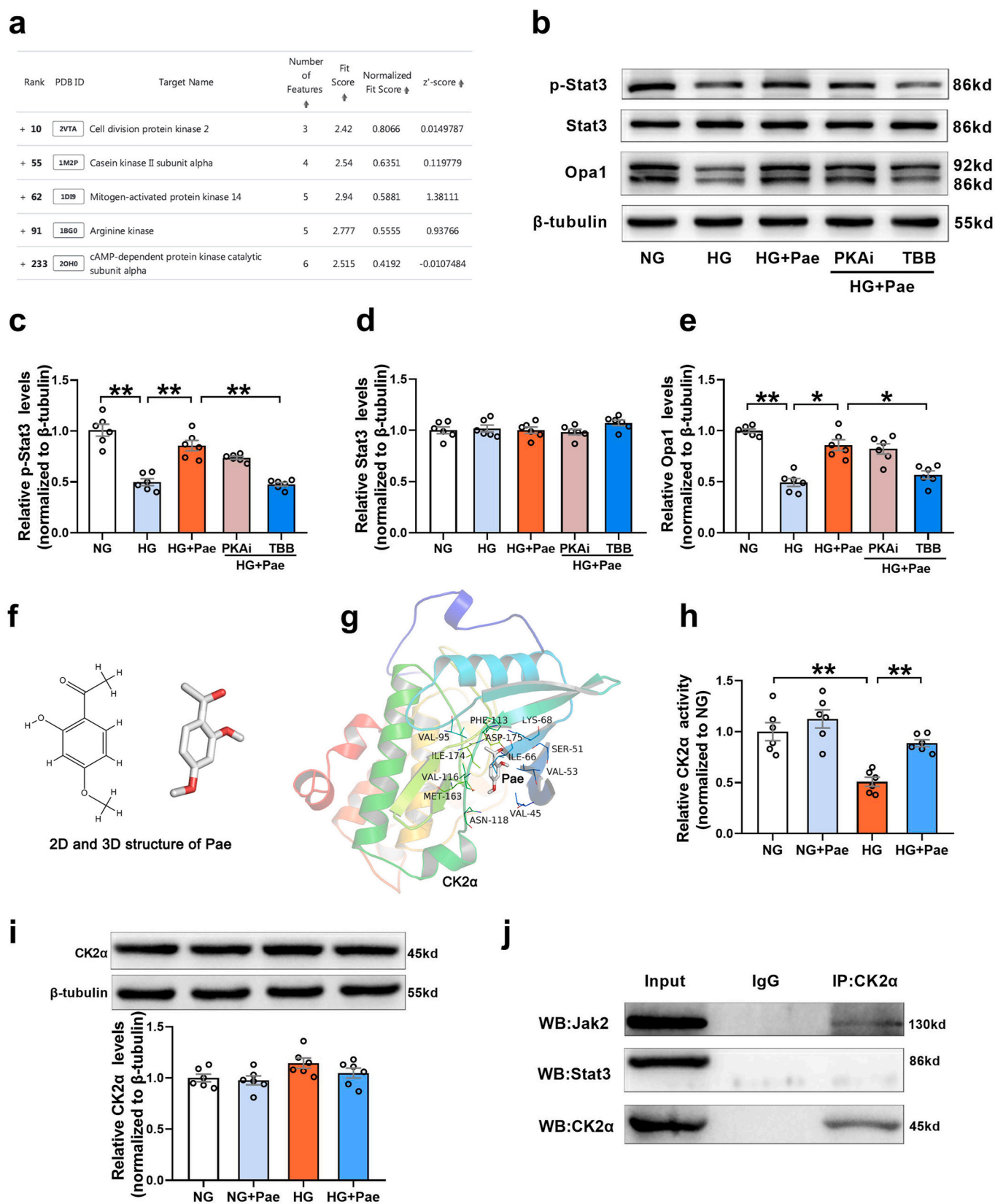


Fig. 8. Pae interacted with CK2 α and restored the activity of CK2 α in high glucose (HG)-treated cardiomyocytes. (a) Listing of potential candidates involved in kinase activity. (b–e) PKA inhibitor (PKAi) or CK2 α inhibitor (TBB) was pre-administered to the cardiomyocytes in the HG + Pae group and then the expression of phosphorylated Stat3 (p-Stat3), total Stat3 and Opa1 were quantified. (f) The 2D and 3D structure of Pae. (g) Binding mode between Pae and CK2 α . CK2 α is represented with the cartoon, and the representative binding residues are indicated by lines. (h) Relative CK2 α activity. (i) Representative blots and quantitative analysis of CK2 α expression. (j) Interaction between CK2 α and Jak2 or Stat3 determined by co-immunoprecipitation. NG, normal glucose (5.5 mmol/L); HG, high glucose (33 mmol/L); Pae, paenonol (100 μ mol/L). $n = 6$ in each group. All data are shown as means \pm SEM. * $P < 0.05$, ** $P < 0.01$.

favorably bind to CK2 α (maximum binding affinity -6.4 kcal/mol, Fig. 8g). The cellular experimental study showed that Pae reversed HG-induced inhibition of CK2 α activity, although Pae did not affect the expression of CK2 α in HG-treated cardiomyocytes (Fig. 8h and i). Pretreatment with the antioxidants NAC (N-acetyl-L-cysteine, 0.5 mmol/L)

or Tempol (4-hydroxy-2,2,6,6-tetramethylpiperidine 1-oxyl, 10 μ mol/L) increased the activity of CK2 α in HG-cultured cardiomyocytes. Pae further elevated CK2 α activity following pretreatment with the antioxidants (Supplementary Fig. S4). Furthermore, co-immunoprecipitation experiments indicated that Jak2, an upstream activator of Stat3, co-

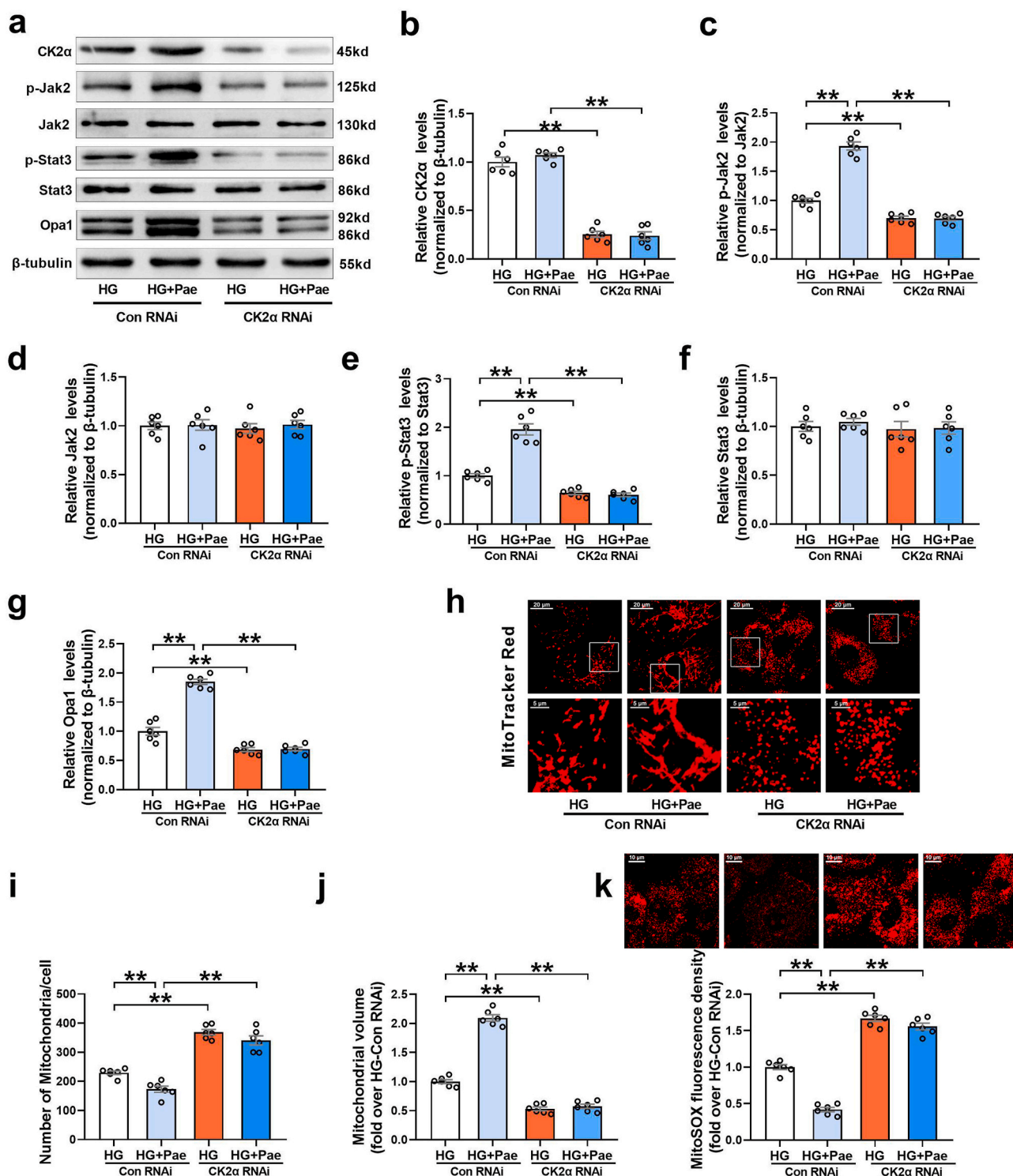


Fig. 9. Knockdown of CK2 α with siRNA blunted the promoting effect of Pae on Jak2 and Stat3 phosphorylation and Opa1-mediated mitochondrial fusion in high glucose (HG)-treated cardiomyocytes. (a-g) Representative blots and quantitative analysis of CK2 α , phosphorylated Jak2 (p-Jak2), Jak2, phosphorylated Stat3 (p-Stat3), Stat3 and Opa1. (h) Representative confocal microscope images of mitochondrial morphology stained by Mitotracker Red. Original magnification $\times 600$. (i) Quantification of mitochondrial number per cell. (j) Quantification of mean mitochondrial volume. (k) Representative images and quantitative analysis of MitoSOX-stained mitochondria-derived superoxide production. HG, high glucose (33 mmol/L); Pae, paeonol (100 μ mol/L). $n = 6$ in each group. All data are shown as means \pm SEM. ** $P < 0.01$. (For interpretation of the references to colour in this figure legend, the reader is referred to the Web version of this article.)

precipitated with endogenous CK2 α , whereas Stat3 did not (Fig. 8j). This suggested that CK2 α may directly interact with Jak2 and subsequently induce the activation of Jak2-Stat3 signaling.

Finally, we investigated whether CK2 α was responsible for enhanced Jak2-Stat3 signaling and Opa1-mediated mitochondrial fusion in response to Pae treatment. As shown in Fig. 9, knockdown of CK2 α with siRNA further inhibited the phosphorylation of Jak2 and Stat3 (Fig. 9a–f), suppressed Opa1-mediated mitochondrial fusion (Fig. 9g–j) and increased mitochondrial oxidative stress (Fig. 9k) in HG-treated cardiomyocytes. Moreover, CK2 α siRNA blunted the upregulating effects of Pae on Jak2 and Stat3 phosphorylation and Opa1-mediated mitochondrial fusion (Fig. 9a–j) as well as largely blocked the inhibitory effects of Pae on mitochondrial oxidative stress (Fig. 9k) in cardiomyocytes. The animal experimental study validated that Pae restored the activity of CK2 α and increased Jak2 and Stat3 phosphorylation in the diabetic hearts (Supplementary Fig. S5). These results above indicated that CK2 α served as a direct target of Pae that activated the Jak2–Stat3 signaling pathway and promoted Opa1-mediated mitochondrial fusion.

4. Discussion

In this study, we demonstrated for the first time that Pae administration inhibits mitochondria-derived oxidative stress and preserves mitochondrial function as well as cardiac performance by promoting Opa1-mediated mitochondrial fusion in DCM *in vivo* and *in vitro*. Mechanistically, using *in vitro* (inhibitor screening and siRNA-based target confirmation) and *in silico* (pharmmapper screening and molecular docking) studies, it is verified that Pae binds to and activates CK2 α that subsequently interacts with Jak2 and induces the phosphorylation and activation of the Jak2-Stat3 signaling, which then binds to the Opa1 promoter to promote Opa1-mediated mitochondrial fusion (Fig. 10). Thus, our study uncovers the detailed molecular mechanism on how Pae promotes mitochondrial fusion and inhibits mitochondrial oxidative stress under diabetic conditions.

Mitochondrial dysfunction associated with excessive ROS production has been recognized to significantly contribute to the development of DCM [41]. Recent studies from our lab and others have demonstrated that mitochondrial fusion is correlated with enhanced mitochondrial function and decreased mitochondrial ROS production [11,42,43]. Therefore, agents with the ability to promote mitochondrial fusion have great potential for inhibiting mitochondrial oxidative stress and protecting against the development of DCM. Previous reports have shown

that Pae has potential as a protective agent in several cardiovascular diseases including atherosclerosis [44], hypertension [45] and myocardial ischemic injury [15], acting mainly via anti-inflammatory mechanisms. Few studies have focused on the role of mitochondria in the protective effects of Pae. Stimulating PGC1 α -regulated mitochondrial biogenesis could increase mitochondrial content and also inhibit mitochondrial ROS production [46,47], which is similar with the protective effects of mitochondrial fusion promotion. Thus, when regarding the protective action of Pae on mitochondria, both mitochondrial biogenesis and mitochondrial fusion has been considered. Our data suggest that Pae inhibits mitochondrial ROS and improves mitochondrial function by promoting Opa1-mediated mitochondrial fusion rather than by stimulating PGC1 α -regulated mitochondrial biogenesis. Moreover, Pae was shown to be effective in protecting against diabetic cardiac complications without significantly affecting blood glucose in the diabetic rats. A previous study by Liu et al. has shown that Pae has a weak glucose-lowering effect [48]. This discrepancy may be due to different animal model. In our study, the diabetic model was induced by relatively high dose of STZ (65 mg/kg). In the study by Liu et al. [48], the diabetic model was induced by high fat/high sucrose feed and relatively low dose of STZ (40 mg/kg). In general, Pae has not been considered as a potent glucose-lowering drug during long time of clinical practice.

In our previous article, M1 has been used as an agonist tool compound to promote mitochondrial fusion [11], whereas its chemical, physical and toxicological properties are so far largely unclear, which limits its application in practice. In contrast, Pae has the advantage that it is already approved and considered safe to use. One novelty of our study is that we have identified an approved drug Pae as a new mitochondrial fusion promoter to protect against diabetic cardiomyopathy. The promotion of mitochondrial fusion may represent a crucial mechanism by which Pae exerts its cardioprotective effects. Moreover, in our previous article [11], the complex mechanisms underlying inhibited Opa1-mediated mitochondrial fusion in diabetic hearts remain unclear. Another novelty of this study is that we have uncovered the detailed molecular mechanism on how Opa1-mediated mitochondrial fusion was inhibited by diabetes and restored by Pae after several times of screening and validation. Our results suggest that inactivated CK2 α -Jak2-Stat3 signaling pathway is account for the reduced transcriptional level of Opa1 and inhibited mitochondrial fusion in diabetic hearts.

During the process of mitochondrial fusion, fusion of the outer mitochondrial membrane is followed by inner membrane fusion. Mfn1

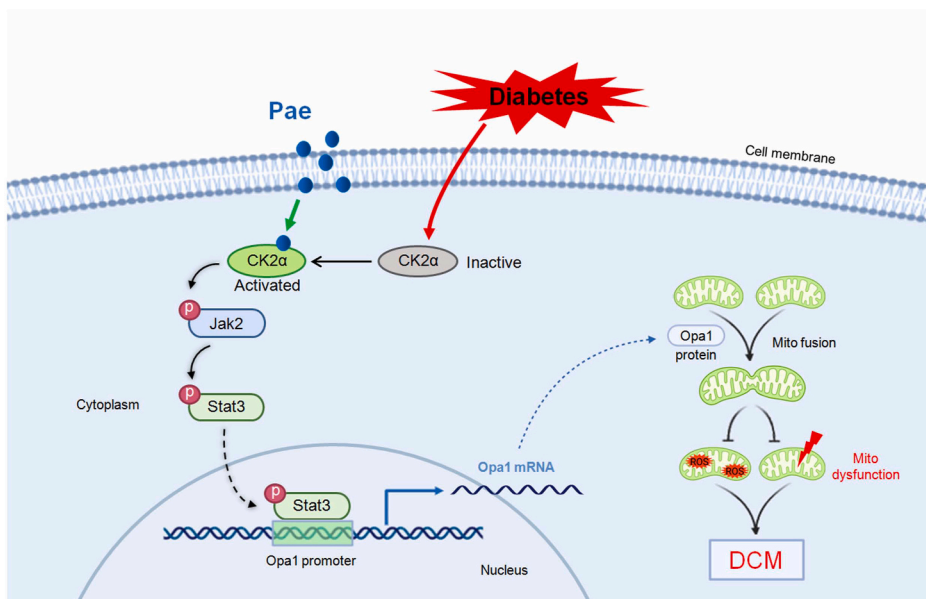


Fig. 10. Schematic figure illustrating that Pae alleviates diabetic cardiomyopathy by promoting Opa1-mediated mitochondrial fusion via activating the CK2 α -Jak2-Stat3 pathway. Pae binds to diabetes-inactivated CK2 α and restores its activity that subsequently interacts with Jak2 and induces the phosphorylation and activation of the Jak2-Stat3 signaling. Activated Stat3 binds to the Opa1 promoter to promote Opa1-mediated mitochondrial fusion. Afterward, Pae-induced upregulation of Opa1 promotes mitochondrial fusion, inhibits mitochondria-derived oxidative stress, preserves mitochondrial function and protects against diabetic cardiomyopathy. Pae, paeonol; Mito, mitochondrial; ROS, reactive oxygen species; DCM, diabetic cardiomyopathy.

and Mfn2 are required for the fusion of the outer mitochondrial membrane. Opa1 is localized to the mitochondrial inner membrane and is a key protein responsible for inner membrane fusion [49]. In the present study, we found that only the expression of Opa1 was markedly lower in the diabetic hearts and in the high glucose-treated cardiomyocytes, whereas the expression of other mitochondrial fusion proteins including Mfn1 and Mfn2 showed no significant change. This may be partly due to insulin deficiency in the STZ-induced diabetic model, since it has been demonstrated that insulin increases the expression of Opa1 in cardiomyocytes without affecting the expression of Mfn1 and Mfn2 [50]. The level of Opa1 protein is regulated by transcriptional regulation and post-translational modifications. Long form and short form of Opa1 could be generated by proteolytic cleavage. The relative contributions of the two different isoforms of Opa1 are diverse. Long form of Opa1 (L-Opa1) is known as the functional variant for fusion between mitochondria, while short form of Opa1 (S-Opa1) is considered as an inactive variant [51,52]. Recently, Yoon and colleagues have interesting work showing that S-Opa1 protects against oxidant-induced cell death [53]. Our study suggests that Opa1 may not be proteolytically cleaved by hyperglycemia or Pae treatment, since long and short forms of Opa1 were not selectively affected by high glucose or Pae. In addition to promoting mitochondrial fusion, Opa1 has been demonstrated to participate in the regulation of mitochondrial cristae morphology, and that this facilitates electron transport and enhances mitochondrial oxidative phosphorylation in the respiratory chain [54,55]. Our study found that cristae density was significantly reduced in the diabetic hearts with decreased Opa1 expression. Knockdown of Opa1 in diabetic hearts blunted the upregulating effects of Pae on cristae density. These results suggest that the protective effects of Opa1 are mediated not only by the fusion of mitochondria but also by the remodeling of mitochondrial cristae.

Despite the known cardioprotective effects of Pae from previous studies [15,44,45], the mechanism of Pae's direct interaction with molecular targets is still largely unknown. An important observation is that we have shown for the first time that Pae binds to CK2 α and then activates the Jak2-Stat3 pathway. As one catalytic subunit of the protein kinase CK2, CK2 α bears most of the sequence and structural features common to holoenzymes [56]. CK2 does not require phosphorylation for its activation [57]. The expression and activity of CK2 are disturbed under many pathophysiological conditions. It has been reported that CK2 activity is decreased in hypertrophic hearts or cardiomyocytes, and oxidative modification results in a dramatic reduction in CK2 activity [58]. In our study, diabetes or high glucose inhibited the activity of CK2 α rather than affecting its expression. Pretreatment with the antioxidants elevated the activity of CK2 α in HG-cultured cardiomyocytes. Pae could further increase CK2 α activity following pretreatment with the antioxidants. The results suggest that the impact of Paeonol on CK2 α activity is not solely due to its antioxidant properties. The interaction between Pae and CK2 α may help to increase its activity.

CK2 exerts anti-apoptotic and anti-hypertrophic effects in cardiomyocytes by phosphorylating the caspase-inhibiting protein ARC [58,59]. A recent study has shown that CK2 protects against oxidative stress by positively regulating NF- κ B/RelA transcription activity in cardiomyoblasts [60]. Our study suggests that CK2 α may promote mitochondrial fusion and exert myocardial protective effects by activating the Jak2-Stat3-Opa1 signaling pathway in the diabetic hearts. Nevertheless, it should be noted that there have been some contradictory results regarding the role of CK2 α in the hearts. Zhou et al. have found that CK2 α promotes the phosphorylation of Mff to facilitate mitochondrial fission and serves as a negative regulator of mitochondrial activity in cardiac ischemia-reperfusion injury [61,62]. This discrepancy may be due to distinct substrates phosphorylated and regulated by CK2 under different pathophysiological situations, since CK2 is a pleiotropic protein kinase acting on more than 300 substrates [56].

It is to be noted that our study has some limitations. First, Pae has

been shown to be an efficient mitochondrial fusion promoter against mitochondrial oxidative injury and resultant DCM exclusively in an STZ-induced animal model of type 1 diabetes and high glucose-treated cardiomyocytes, which may not entirely represent the complex conditions caused by diabetes. Further investigation is needed to determine whether the mitochondrial fusion-promoting and cardioprotective effects of Pae could be applied to other diabetic models. Second, the role of CK2 α -Stat3 signaling in the promoting effects of Pae on mitochondrial fusion was mainly explored *in vitro* using CK2 α or Stat3 siRNA. Knockdown of CK2 α or Stat3 in the heart *in vivo* will be helpful to verify the promoting action of Pae on Opa1-mediated mitochondrial fusion via a CK2 α -Stat3-dependent way. Third, although Opa1 is required for the mitochondrial fusion-promoting effect of Pae in our study, it should be noted that Opa1 may not be the only key molecule involved in Pae-induced cardioprotection. A complex array of signaling pathways indeed participates in the therapeutic effects of Pae and future work will be needed to clarify this issue. Despite these limitations, we believe that our findings provide important novel insights for understanding the mitochondrial protective effects of Pae and the underlying mechanisms.

In summary, our study provides novel evidence indicating that Pae promotes mitochondrial fusion and protects against diabetic cardiomyopathy at least partially by upregulating Opa1 expression, a process in which Pae interacts with CK2 α and restores its kinase activity that subsequently increasing Jak2-Stat3 phosphorylation and enhancing the transcriptional level of Opa1. These findings suggest that Pae or promotion of mitochondrial fusion might be a new potential option for the treatment of patients with DCM.

Fundings

This study was supported by the grants from National Natural Science Foundation of China (No. 82070387, No. 81970316, No. 82070051, No. 81770243, No. 82111530058), Key Research and Development Plan of Shaanxi (No. 2021SF-141), Innovation Capability Support Program of Shaanxi (No. 2019KJXX-084), the Fundamental Research Funds for the Central Universities (No. xzy012019115) and Russian Foundation of Basic Research Grant (No. 21-515-53003).

Declaration of competing interest

Authors declare no competing interests.

Appendix A. Supplementary data

Supplementary data to this article can be found online at <https://doi.org/10.1016/j.redox.2021.102098>.

References

- [1] M. Knapp, X. Tu, R. Wu, Vascular endothelial dysfunction, a major mediator in diabetic cardiomyopathy, *Acta Pharmacol. Sin.* 40 (1) (2019) 1–8.
- [2] V. Chavali, S.C. Tyagi, P.K. Mishra, Predictors and prevention of diabetic cardiomyopathy, *Diabetes Metab Syndr Obes* 6 (2013) 151–160.
- [3] K. Huynh, B.C. Bernardo, J.R. McMullen, R.H. Ritchie, Diabetic cardiomyopathy: mechanisms and new treatment strategies targeting antioxidant signaling pathways, *Pharmacol. Ther.* 142 (3) (2014) 375–415.
- [4] C. Tribouilloy, D. Rusinaru, H. Mahjoub, J.M. Tardiere, L. Kesri-Tardiere, S. Godard, M. Peltier, Prognostic impact of diabetes mellitus in patients with heart failure and preserved ejection fraction: a prospective five-year study, *Heart* 94 (11) (2008) 1450–1455.
- [5] J. Marin-Garcia, A.T. Akhmedov, Mitochondrial dynamics and cell death in heart failure, *Heart Fail. Rev.* 21 (2) (2016) 123–136.
- [6] N. Kaludercic, F. Di Lisa, Mitochondrial ROS formation in the pathogenesis of diabetic cardiomyopathy, *Front Cardiovasc Med* 7 (2020) 12.
- [7] F.F. Jubaidi, S. Zainalabidin, V. Mariappan, S.B. Budin, Mitochondrial dysfunction in diabetic cardiomyopathy: the possible therapeutic roles of phenolic acids, *Int. J. Mol. Sci.* 21 (17) (2020) 6043.
- [8] T. Yu, S.S. Sheu, J.L. Robotham, Y. Yoon, Mitochondrial fission mediates high glucose-induced cell death through elevated production of reactive oxygen species, *Cardiovasc. Res.* 79 (2) (2008) 341–351.

- [9] J. Marin-Garcia, A.T. Akhmedov, G.W. Moe, Mitochondria in heart failure: the emerging role of mitochondrial dynamics, *Heart Fail. Rev.* 18 (4) (2013) 439–456.
- [10] M. Ding, N. Feng, D. Tang, J. Feng, Z. Li, M. Jia, Z. Liu, X. Gu, Y. Wang, F. Fu, J. Pei, Melatonin prevents Drp1-mediated mitochondrial fission in diabetic hearts through SIRT1-PGC1 α pathway, *J. Pineal Res.* 65 (2) (2018), e12491.
- [11] M. Ding, C. Liu, R. Shi, M. Yu, K. Zeng, J. Kang, F. Fu, M. Mi, Mitochondrial fusion promoter restores mitochondrial dynamics balance and ameliorates diabetic cardiomyopathy in an optic atrophy 1-dependent way, *Acta Physiol.* 229 (1) (2020), e13428.
- [12] Y. Qin, A. Li, B. Liu, W. Jiang, M. Gao, X. Tian, G. Gong, Mitochondrial fusion mediated by fusion promotion and fission inhibition directs adult mouse heart function toward a different direction, *Faseb. J.* 34 (1) (2020) 663–675.
- [13] L. Zhang, D.C. Li, L.F. Liu, Paeonol: pharmacological effects and mechanisms of action, *Int. Immunopharm.* 72 (2019) 413–421.
- [14] I.T. Nizamutdinova, Y.C. Jin, J.S. Kim, M.H. Yean, S.S. Kang, Y.S. Kim, J.H. Lee, H. G. Seo, H.J. Kim, K.C. Chang, Paeonol and paeoniflorin, the main active principles of *Paonia albiflora*, protect the heart from myocardial ischemia/reperfusion injury in rats, *Planta Med.* 74 (1) (2008) 14–18.
- [15] H. Li, F. Song, L.R. Duan, J.J. Sheng, Y.H. Xie, Q. Yang, Y. Chen, Q.Q. Dong, B. L. Zhang, S.W. Wang, Paeonol and danshensu combination attenuates apoptosis in myocardial infarcted rats by inhibiting oxidative stress: roles of Nrf2/HO-1 and PI3K/Akt pathway, *Sci. Rep.* 6 (2016) 23693.
- [16] X. Wang, G. Zhu, S. Yang, X. Wang, H. Cheng, F. Wang, X. Li, Q. Li, Paeonol prevents excitotoxicity in rat pheochromocytoma PC12 cells via downregulation of ERK activation and inhibition of apoptosis, *Planta Med.* 77 (15) (2011) 1695–1701.
- [17] M. Ding, J. Ning, N. Feng, Z. Li, Z. Liu, Y. Wang, Y. Wang, X. Li, C. Huo, X. Jia, R. Xu, F. Fu, X. Wang, J. Pei, Dynamine-related protein 1-mediated mitochondrial fission contributes to post-traumatic cardiac dysfunction in rats and the protective effect of melatonin, *J. Pineal Res.* 64 (1) (2018), e12447.
- [18] Z.G. Ma, Y.P. Yuan, S.C. Xu, W.Y. Wei, C.R. Xu, X. Zhang, Q.Q. Wu, H.H. Liao, J. Ni, Q.Z. Tang, CTRP3 attenuates cardiac dysfunction, inflammation, oxidative stress and cell death in diabetic cardiomyopathy in rats, *Diabetologia* 60 (6) (2017) 1126–1137.
- [19] F. Xu, H. Xiao, R. Liu, Y. Yang, M. Zhang, L. Chen, Z. Chen, P. Liu, H. Huang, Paeonol ameliorates glucose and lipid metabolism in experimental diabetes by activating Akt, *Front. Pharmacol.* 10 (2019) 261.
- [20] L. Zhang, Z. Chen, W. Gong, Y. Zou, F. Xu, L. Chen, H. Huang, Paeonol ameliorates diabetic renal fibrosis through promoting the activation of the Nrf2/ARE pathway via up-regulating Sirt1, *Front. Pharmacol.* 9 (2018) 512.
- [21] X. Wang, Y. Shen, S. Wang, S. Li, W. Zhang, X. Liu, L. Lai, J. Pei, H. Li, PharmMapper 2017 update: a web server for potential drug target identification with a comprehensive target pharmacophore database, *Nucleic Acids Res.* 45 (W1) (2017) 356–360.
- [22] X. Liu, S. Ouyang, B. Yu, Y. Liu, K. Huang, J. Gong, S. Zheng, Z. Li, H. Li, H. Jiang, PharmMapper server: a web server for potential drug target identification using pharmacophore mapping approach, *Nucleic Acids Res.* 38 (Web Server issue) (2010) 609–614.
- [23] Z. Li, X. Wu, L. Jia, J. Li, R. Zhang, H. Tang, Z. Li, H. Bu, C. Shen, Design and synthesis of novel 2-arylbenzimidazoles as selective mutant isocitrate dehydrogenase 2 R140Q inhibitors, *Bioorg. Med. Chem. Lett.* 30 (9) (2020) 127070.
- [24] Z. Li, L. Jia, H. Tang, Y. Shen, C. Shen, Synthesis and biological evaluation of geldanamycin–ferulic acid conjugate as a potent Hsp90 inhibitor, *RSC Adv.* 9 (72) (2019) 42509–42515.
- [25] L. Ji, F. Fu, L. Zhang, W. Liu, X. Cai, L. Zhang, Q. Zheng, H. Zhang, F. Gao, Insulin attenuates myocardial ischemia/reperfusion injury via reducing oxidative/nitrative stress, *Am. J. Physiol. Endocrinol. Metab.* 298 (4) (2010) E871–E880.
- [26] N. Liu, X. Feng, W. Wang, X. Zhao, X. Li, Paeonol protects against TNF- α -induced proliferation and cytokine release of rheumatoid arthritis fibroblast-like synoviocytes by upregulating FOXO3 through inhibition of miR-155 expression, *Inflamm. Res.* 66 (7) (2017) 603–610.
- [27] Q. Wang, X. Xu, Z. Kang, Z. Zhang, Y. Li, Paeonol prevents IL-1 β -induced inflammatory response and degradation of type II collagen in human primary chondrocytes, *Artif Cells Nanomed Biotechnol* 47 (1) (2019) 2139–2145.
- [28] X. Wu, H. Chen, X. Chen, Z. Hu, Determination of paeonol in rat plasma by high-performance liquid chromatography and its application to pharmacokinetic studies following oral administration of Moutan cortex decoction, *Biomed. Chromatogr.* 17 (8) (2003) 504–508.
- [29] J. Li, Z.Q. Xu, L. Bao, Z.C. Li, J.X. Qu, Protective effects of paeonol on cardiovascular complications in diabetes mellitus involves modulation of PI3K/Akt-GSK-3 β signalling, regulation of protease-activated receptor-1 expressions and down-regulation of inflammatory mediators, *Bangladesh J. Pharmacol.* 10 (4) (2015) 903–916.
- [30] R.Q. Chang, J. Shao, Y.H. Meng, J. Wang, D.J. Li, M.Q. Li, Decidual RANKL/RANK interaction promotes the residence and polarization of TGF- β 1-producing regulatory gammadelta T cells, *Cell Death Dis.* 10 (2) (2019) 113.
- [31] S. Lei, W. Su, Z.Y. Xia, Y. Wang, L. Zhou, S. Qiao, B. Zhao, Z. Xia, M.G. Irwin, Hyperglycemia-induced oxidative stress abrogates remifentanyl preconditioning-mediated cardioprotection in diabetic rats by impairing Caveolin-3-modulated PI3K/Akt and JAK2/STAT3 signaling, *Oxid Med Cell Longev* (2019) (2019) 9836302.
- [32] M. Florian, M. Jankowski, J. Gutkowska, Oxytocin increases glucose uptake in neonatal rat cardiomyocytes, *Endocrinology* 151 (2) (2010) 482–491.
- [33] V. Leidgens, J. Proske, L. Rauer, S. Moeckel, K. Renner, U. Bogdahn, M. J. Riemenschneider, M. Proescholdt, A. Vollmann-Zwerenz, P. Hau, C. Seliger, Stattic and metformin inhibit brain tumor initiating cells by reducing STAT3-phosphorylation, *Oncotarget* 8 (5) (2017) 8250–8263.
- [34] Y. Wang, W. Zang, S. Ji, J. Cao, C. Sun, Three polymethoxyflavones purified from ougan (*Citrus reticulata* Cv. *Suavissima*) inhibited LPS-induced NO elevation in the Neurogia BV-2 cell line via the JAK2/STAT3 pathway, *Nutrients* 11 (4) (2019) 791.
- [35] D.A. Rosen, S.M. Seki, A. Fernandez-Castaneda, R.M. Beiter, J.D. Eccles, J. A. Woodfolk, A. Gaultier, Modulation of the sigma-1 receptor-IRE1 pathway is beneficial in preclinical models of inflammation and sepsis, *Sci. Transl. Med.* 11 (478) (2019) 5266.
- [36] Y.M. Lee, J.P. Park, K.T. Lim, S.J. Lee, Intestinal epithelial cell apoptosis due to a hemolytic toxin from *Vibrio vulnificus* and protection by a 36kDa glycoprotein from *Rhus verniciflua* Stokes, *Food Chem. Toxicol.* 125 (2019) 46–54.
- [37] J.Y. Kim, Y.M. Lee, D.W. Kim, T. Min, S.J. Lee, Nanosphere loaded with curcumin inhibits the gastrointestinal cell death signaling pathway induced by the foodborne pathogen *vibrio vulnificus*, *Cells* 9 (3) (2020) 631.
- [38] A. Gyawali, S. Krol, Y.S. Kang, Involvement of a novel organic cation transporter in paeonol transport across the blood-brain barrier, *Biomol Ther (Seoul)*. 27 (3) (2019) 290–301.
- [39] E.C. Arakel, S. Brandenburg, K. Uchida, H. Zhang, Y.W. Lin, T. Kohl, B. Schrul, M. S. Sulkin, I.R. Efimov, C.G. Nichols, S.E. Lehnart, B. Schwappach, Tuning the electrical properties of the heart by differential trafficking of K_{ATP} ion channel complexes, *J. Cell Sci.* 127 (Pt 9) (2014) 2106–2119.
- [40] S. Sarno, H. Reddy, F. Meggio, M. Ruzzeno, S.P. Davies, A. Donella-Deana, D. Shugar, L.A. Pinna, Selectivity of 4,5,6,7-tetrabromobenzotriazole, an ATP site-directed inhibitor of protein kinase CK2 (‘casein kinase-2’), *FEBS Lett.* 496 (1) (2001) 44–48.
- [41] J.G. Duncan, Mitochondrial dysfunction in diabetic cardiomyopathy, *Biochim. Biophys. Acta* 1813 (7) (2011) 1351–1359.
- [42] L. Hu, M. Ding, D. Tang, E. Gao, C. Li, K. Wang, B. Qi, J. Qiu, H. Zhao, P. Chang, F. Fu, Y. Li, Targeting mitochondrial dynamics by regulating Mfn2 for therapeutic intervention in diabetic cardiomyopathy, *Theranostics* 9 (13) (2019) 3687–3706.
- [43] M. Forte, L. Schirone, P. Ameri, C. Basso, D. Catalucci, J. Modica, C. Chimenti, L. Crotti, G. Frati, S. Rubattu, G.G. Schiattarella, D. Torella, C. Perrino, C. Indolfi, S. Sciarretta, The role of mitochondrial dynamics in cardiovascular diseases, *Br. J. Pharmacol.* 178 (10) (2021) 2060–2076.
- [44] H. Li, M. Dai, W. Jia, Paeonol attenuates high-fat-diet-induced atherosclerosis in rabbits by anti-inflammatory activity, *Planta Med.* 75 (1) (2009) 7–11.
- [45] J.Y. Zhang, L. Zhao, Y.K. Li, W.L. Weng, [Effect of paeonol on blood pressure and blood flow in artery of spontaneously hypertensive rats and its mechanisms related on vasomotion], *Zhongguo Zhongyao Zazhi* 40 (24) (2015) 4903–4907.
- [46] R.C. Scarpulla, Metabolic control of mitochondrial biogenesis through the PGC-1 family regulatory network, *Biochim. Biophys. Acta* 1813 (7) (2011) 1269–1278.
- [47] W. Di, J. Lv, S. Jiang, C. Lu, Z. Yang, Z. Ma, W. Hu, Y. Yang, B. Xu, PGC-1: the energetic regulator in cardiac metabolism, *Curr. Issues Mol. Biol.* 28 (2018) 29–46.
- [48] J. Liu, S. Wang, L. Feng, D. Ma, Q. Fu, Y. Song, X. Jia, S. Ma, Hypoglycemic and antioxidant activities of paeonol and its beneficial effect on diabetic encephalopathy in streptozotocin-induced diabetic rats, *J. Med. Food* 16 (7) (2013) 577–586.
- [49] S.A. Detmer, D.C. Chan, Functions and dysfunctions of mitochondrial dynamics, *Nat. Rev. Mol. Cell Biol.* 8 (11) (2007) 870–879.
- [50] V. Parra, H.E. Verdejo, M. Iglewski, A. Del Campo, R. Troncoso, D. Jones, Y. Zhu, J. Kuzmich, C. Pennanen, C. Lopez-Crisosto, F. Jana, J. Ferreira, E. Nogueira, M. Chiong, D.A. Bernlohr, A. Klip, J.A. Hill, B.A. Rothermel, E.D. Abel, A. Zorzano, S. Lavandro, Insulin stimulates mitochondrial fusion and function in cardiomyocytes via the Akt-mTOR-NF κ B-Opa-1 signaling pathway, *Diabetes* 63 (1) (2014) 75–88.
- [51] S.M. Adaniya, O.U. J. M.W. Cypress, Y. Kusakari, B.S. Jhun, Posttranslational modifications of mitochondrial fission and fusion proteins in cardiac physiology and pathophysiology, *Am. J. Physiol. Cell Physiol.* 316 (5) (2019) C583–C604.
- [52] N. Ishihara, Y. Fujita, T. Oka, K. Mihara, Regulation of mitochondrial morphology through proteolytic cleavage of OPA1, *EMBO J.* 25 (13) (2006) 2966–2977.
- [53] H. Lee, S.B. Smith, S.S. Sheu, Y. Yoon, The short variant of optic atrophy 1 (OPA1) improves cell survival under oxidative stress, *J. Biol. Chem.* 295 (19) (2020) 6543–6560.
- [54] S. Cipolat, T. Rudka, D. Hartmann, V. Costa, L. Serneels, K. Craessaerts, K. Metzger, C. Frezza, W. Annaert, L. D’Adamo, C. Derks, T. Dejaegere, L. Pellegrini, R. D’Hooge, L. Scorrano, B. De Strooper, Mitochondrial rhomboid PARL regulates cytochrome c release during apoptosis via OPA1-dependent cristae remodeling, *Cell* 126 (1) (2006) 163–175.
- [55] S.B. Ong, S.B. Kalkhoran, S. Hernandez-Resendiz, P. Samangouei, S.G. Ong, D. J. Hausenloy, Mitochondrial-shaping proteins in cardiac health and disease - the long and the short of it!, *Cardiovasc. Drugs Ther.* 31 (1) (2017) 87–107.
- [56] R. Battistutta, Protein kinase CK2 in health and disease: structural bases of protein kinase CK2 inhibition, *Cell. Mol. Life Sci.* 66 (11–12) (2009) 1868–1889.

- [57] R. Battistutta, G. Lolli, Structural and functional determinants of protein kinase CK2alpha: facts and open questions, *Mol. Cell. Biochem.* 356 (1–2) (2011) 67–73.
- [58] I. Murtaza, H.X. Wang, X. Feng, N. Alenina, M. Bader, B.S. Prabhakar, P.F. Li, Down-regulation of catalase and oxidative modification of protein kinase CK2 lead to the failure of apoptosis repressor with caspase recruitment domain to inhibit cardiomyocyte hypertrophy, *J. Biol. Chem.* 283 (10) (2008) 5996–6004.
- [59] P.F. Li, J. Li, E.C. Muller, A. Otto, R. Dietz, R. von Harsdorf, Phosphorylation by protein kinase CK2: a signaling switch for the caspase-inhibiting protein ARC, *Mol. Cell* 10 (2) (2002) 247–258.
- [60] S. Schaefer, B. Guerra, Protein kinase CK2 regulates redox homeostasis through NF-kappaB and Bcl-xL in cardiomyoblasts, *Mol. Cell. Biochem.* 436 (1–2) (2017) 137–150.
- [61] H. Zhou, J. Wang, P. Zhu, H. Zhu, S. Toan, S. Hu, J. Ren, Y. Chen, NR4A1 aggravates the cardiac microvascular ischemia reperfusion injury through suppressing FUNDC1-mediated mitophagy and promoting Mif-required mitochondrial fission by CK2alpha, *Basic Res. Cardiol.* 113 (4) (2018) 23.
- [62] H. Zhou, P. Zhu, J. Wang, H. Zhu, J. Ren, Y. Chen, Pathogenesis of cardiac ischemia reperfusion injury is associated with CK2alpha-disturbed mitochondrial homeostasis via suppression of FUNDC1-related mitophagy, *Cell Death Differ.* 25 (6) (2018) 1080–1093.